Gottfried Spelsberg-Korspeter
e-mail: speko@dyn.tu-darmstadt.de

Daniel Hochlenert
e-mail: hochlenert@dyn.tu-darmstadt.de

Oleg N. Kirillov[1]
e-mail: kirillov@dyn.tu-darmstadt.de

Peter Hagedorn
e-mail: peter.hagedorn@dyn.tu-darmstadt.de

Department of Mechanical Engineering,
Dynamics and Vibrations Group,
Technische Universität Darmstadt,
Hochschulstrasse 1,
64289 Darmstadt, Germany

In- and Out-of-Plane Vibrations of a Rotating Plate With Frictional Contact: Investigations on Squeal Phenomena

Rotating plates are used as a main component in various applications. Their vibrations are mainly unwanted and interfere with the functioning of the complete system. The present paper investigates the coupling of disk (in-plane) and plate (out-of-plane) vibrations of a rotating annular Kirchhoff plate in the presence of a distributed frictional loading on its surface. The boundary value problem is derived from the basics of the theory of elasticity using Kirchhoff's assumptions. This results in precise information about the coupling between the disk and the plate vibrations under the action of frictional forces. At the same time we obtain a new model, which is efficient for analytical treatment. Approximations to the stability boundaries of the system are calculated using a perturbation approach. In the last part of the paper nonlinearities are introduced leading to limit cycles due to self-excited vibrations. [DOI: 10.1115/1.3112734]

1 Introduction

Rotating plates occur in many technical applications such as computer hard drives, turbines, saws, clutches, and disk brakes. In some of these applications squeal phenomena arise due to instabilities of the system, of which the plate plays an essential role. Those effects are usually unwanted. In many cases the instabilities and therefore the squeal phenomena are due to self-excited vibrations originating from frictional loads acting on the surface of the rotating plate. The present paper deals with rotating plates in contact with idealized friction pads.

Various questions related to rotating plates have been extensively investigated in literature. Probably among the first publications in the field were the papers by Lamb and Southwell [1,2], giving the equations of motion of a rotating Kirchhoff plate taking into account the effect of centrifugal stiffening due to membrane stresses. Another approach is to derive the equations of motion for plates using the corresponding kinematic assumptions in the basic equations of the theory of elasticity (see, e.g., Ref. [3]). For spinning disks, different kinds of modeling strategies are reviewed and compared in Refs. [4,5].

It is well known that the linear disk and plate equations are decoupled. Whereas a derivation from the linear deformation gradient yields linear equations, disk and plate equations are coupled through nonlinear terms when the nonlinear deformation gradient is used [3]. If the plate interacts with other mechanical systems, coupling between disk and plate vibrations is possible even when using a geometrically linearized theory. In our paper, the plate interacts with idealized friction pads, which may lead to such a type of coupling. Especially concerning the problem of brake squeal, where only small deformations occur and therefore the geometrically linearized theory seems to be appropriate, the influence of the disk vibrations to the plate vibrations has not been fully investigated, although experimental results seem to indicate this type of coupling [6]. An overview directly related to the present paper, i.e., friction induced instabilities in rotating disks, is given by Mottershead [7].

Ono et al. [8] considered a rotating plate in frictional contact with a transverse dynamical system as a model of a computer hard drive. Centrifugal and aeroelastic effects were taken into account, as required by typical rotational speeds of hard drives. In the context of brake squeal Ouyang and Mottershead [9] investigated a stationary plate loaded by a rotating friction couple. These results explain the instabilities occurring in a rotating plate, provided the effect of centrifugal stiffening can be neglected. It has, however, to be said that the model contains slight inconsistencies regarding the modeling of the frictional contact, since normal and friction forces are not perpendicular at all times in this analysis. A broad overview of models related to the squeal of disk brakes is given in Ref. [10], and an overview about the physical phenomena in friction induced vibrations is given in Ref. [11].

Nevertheless, none of the papers cited above comment on the possible coupling between disk (in-plane) and plate (out-of-plane) vibrations, in general, and due to contact forces originating from a frictional contact, in particular. The paper by Tseng and Wickert [12] aims in this direction by investigating a rotating plate loaded by a given shear stress acting like a follower force on the surface of the plate. Following this approach it is possible to calculate the membrane in-plane stresses in a first step and then introduce them into the plate equations in a second step. Since the forces acting on the plate are modeled as a given shear stress their magnitude does not depend on the transverse displacement of the plate, which excludes additional coupling effects of the in- and out-of-plane vibrations.

In the present paper we propose a model of a disk brake, which takes into account in- and out-of-plane motions of the brake rotor, and its interaction with friction pads. Using Kirchhoff's kinematical assumptions for the rotating continuum in interaction with friction pads we derive a new boundary value problem from the basics of the theory of elasticity using the variational approach. The consistent contact formulation based on Coulomb's law of friction given by Hochlenert et al. [13] is retained and extended to distributed contact. Concentrating on the coupling effect of the pads, which has not been investigated in literature, we prefer to work with the linear deformation gradient. For completeness we show in Sec. 4.4 that working with the nonlinear deformation

[1]Visiting from the Institute of Mechanics, Moscow State Lomonosov University, Michurinskii Prospect 1, 119192 Moscow, Russia.

Contributed by the Applied Mechanics Division of ASME for publication in the JOURNAL OF APPLIED MECHANICS. Manuscript received June 15, 2007; final manuscript received February 3, 2009; published online April 22, 2009. Review conducted by Arvind Raman.

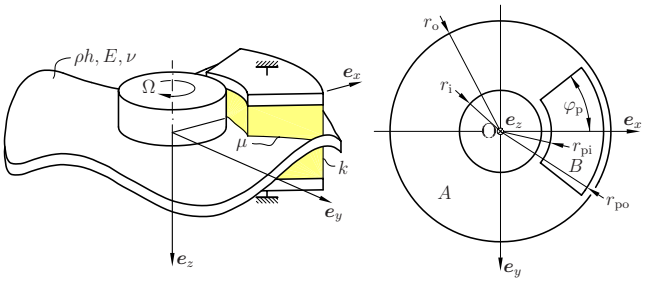

Fig. 1 Kirchhoff plate in distributed frictional contact

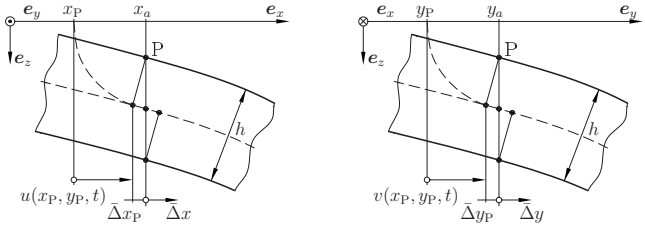

Fig. 3 Contact kinematics

gradient essentially introduces the effect of centrifugal stiffening into the model but does not yield an additional coupling in the linearized equations. Neglecting in-plane degrees of freedom of the pads we investigate whether there is a coupling induced by the out-of-plane degrees of freedom of the pads. It is established that the linearized equations for the in- and out-of-plane motions are decoupled and thus can be solved independently. This justifies the discretization approach described in Ref. [13]. The mathematical model presented is efficient to handle even analytically using perturbation techniques and at the same time it is rather flexible allowing for various extensions.

A perturbation approach developed in Refs. [14,15] is used to approximate the stability boundaries of the present model. In this context the terms originating from the frictional load are considered as perturbations to the problem. The equations of motion of the unperturbed problem corresponding to the out-of-plane vibrations can be written as infinitely many uncoupled two-dimensional systems, making it possible to derive approximations to the stability boundaries by considering these reduced systems only. New explicit perturbation formulas are derived, which prove to be an efficient tool in the stability analysis.

In the last part of the paper a reduced nonlinear model with parameters corresponding to a standard disk brake is studied. It is shown that depending on the parameters, the system can get unstable either via a sub- or a supercritical Hopf bifurcation. The latter one serves as an explanation for the nonlinear effects observed in laboratory experiments with a standard disk brake that to the extent of the authors' knowledge so far have not been investigated.

2 Derivation of the Mathematical Model

Consider a rotating Kirchhoff plate in frictional contact with idealized brake pads, as shown in Fig. 1. The pads are composed of massless pins in contact with the plate at a single point. In the following we will refer to this as a pointwise elastic model. For simplicity the pins are assumed to have identical characteristics. The model, however, can easily be extended to take into account a nonuniform distribution of the load among the pins. In Fig. 2 the plate is in contact with a single pair of pins. For the derivation of the equations of motion we have to consider the kinematics of the problem and the forcing terms arising due to the pads.

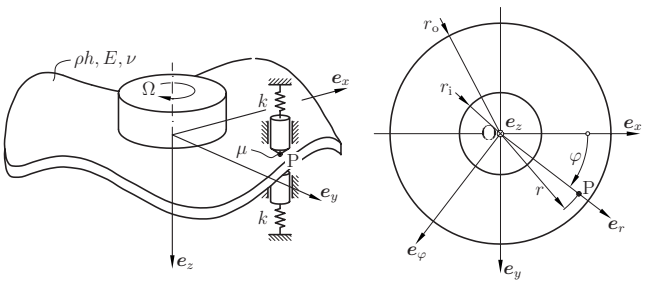

Fig. 2 Kirchhoff plate in pointwise frictional contact

2.1 Kinematics. As usual in Kirchhoff plate theory we assume the following.

- Transverse normal stress can be neglected, i.e., $\sigma_z=0$.
- Material points located on a normal to the neutral plane in the undeformed configuration and in the deformed configuration will be located on one and the same normal to the deformed neutral plane; moreover, the segment formed by these normals is inextensible.

A point on the neutral plane of the plate with the position vector $\boldsymbol{p}_{M0}=x\boldsymbol{e}_x+y\boldsymbol{e}_y$ in the undeformed configuration experiences the displacement

$$\boldsymbol{u}_M = u(x,y,t)\boldsymbol{e}_x + v(x,y,t)\boldsymbol{e}_y + w(x,y,t)\boldsymbol{e}_z \tag{1}$$

and its position vector in the deformed configuration is given by

$$\boldsymbol{p}_M(x,y,t) = (x+u(x,y,t))\boldsymbol{e}_x + (y+v(x,y,t))\boldsymbol{e}_y + w(x,y,t)\boldsymbol{e}_z \tag{2}$$

According to the Kirchhoff assumption the unit normal vector at a point of the neutral plane is given by

$$\boldsymbol{e}_\nabla(x,y,t) = \frac{\dfrac{\partial \boldsymbol{p}_M}{\partial x}\times\dfrac{\partial \boldsymbol{p}_M}{\partial y}}{\left\|\dfrac{\partial \boldsymbol{p}_M}{\partial x}\times\dfrac{\partial \boldsymbol{p}_M}{\partial y}\right\|} \tag{3}$$

and hence a point on the plate surface is given by

$$\boldsymbol{p}(x,y,t) = (x+u(x,y,t))\boldsymbol{e}_x + (y+v(x,y,t))\boldsymbol{e}_y + w(x,y,t)\boldsymbol{e}_z - \frac{h}{2}\boldsymbol{e}_\nabla(x,y,t) \tag{4}$$

The displacement vector of an arbitrary point of the plate is therefore

$$\boldsymbol{u}(x,y,z,t) = \boldsymbol{u}_M(x,y,t) + z(\boldsymbol{e}_\nabla(x,y,t) - \boldsymbol{e}_z) \tag{5}$$

which can be expanded in a Taylor series with respect to u, v, and w to arbitrary order. The linearized expression reads

$$\boldsymbol{u}(x,y,z,t) = (u - zw_{,x})\boldsymbol{e}_x + (v - zw_{,y})\boldsymbol{e}_y + w\boldsymbol{e}_z \tag{6}$$

When differentiating Eq. (2) with respect to time we have to consider $\dot{x}=-\Omega y$ and $\dot{y}=\Omega x$ due to the rotation of the plate, which will be important for the inertia terms arising in the equations of motion.

When considering the point on the surface of the plate currently in contact with a certain pin belonging to the pad we have to calculate its positions x_P and y_P as shown in Fig. 3. From geometrical considerations it is seen that

$$\bar{\Delta}x_P = -\frac{h}{2}\sin(\arctan w_{,x}(x_a+\bar{\Delta}x_P, y_a+\bar{\Delta}y_P, t))$$

$$= -\frac{h}{2}\frac{w_{,x}(x_a+\bar{\Delta}x_P, y_a+\bar{\Delta}y_P, t)}{\sqrt{1+w_{,x}(x_a+\bar{\Delta}x_P, y_a+\bar{\Delta}y_P, t)^2}}$$

$$\bar{\Delta}y_P = -\frac{h}{2}\sin(\arctan w_{,y}(x_a+\bar{\Delta}x_P, y_a+\bar{\Delta}y_P, t))$$

$$= -\frac{h}{2}\frac{w_{,y}(x_a+\bar{\Delta}x_P, y_a+\bar{\Delta}y_P, t)}{\sqrt{1+w_{,y}(x_a+\bar{\Delta}x_P, y_a+\bar{\Delta}y_P, t)^2}}$$

where $w_{,x}$ means differentiation of the function w with respect to x. These are fixed point equations of the type

$$(\bar{\Delta}x_P^{k+1}, \bar{\Delta}y_P^{k+1})^T = \boldsymbol{g}(\bar{\Delta}x_P^k, \bar{\Delta}x_P^k) \quad \text{with} \quad \bar{\Delta}x_P^0 = 0, \quad \bar{\Delta}y_P^0 = 0 \tag{7}$$

Since $w_{,x}$ and $w_{,y}$ are small compared with unity, the Banach fixed point theorem is applicable and Eq. (7) can be solved to arbitrary precision.

We can now calculate $x_P = x_a + \Delta x_P$ and $y_P = y_a + \Delta y_P$ where

$$\Delta x_P = \bar{\Delta}x_P + u(x_P, y_P, t) \tag{8}$$

$$= -\frac{h}{2}\frac{w_{,x}(x_P, y_P, t)}{\sqrt{1+w_{,x}(x_P, y_P, t)^2}} + u(x_P, y_P, t) \tag{9}$$

$$\Delta y_P = \bar{\Delta}y_P + v(x_P, y_P, t) \tag{10}$$

$$= -\frac{h}{2}\frac{w_{,y}(x_P, y_P, t)}{\sqrt{1+w_{,y}(x_P, y_P, t)^2}} + v(x_P, y_P, t) \tag{11}$$

are again fixed point equations that can be solved to arbitrary precision. In the linear case, however, we have

$$\Delta x_P = -\frac{h}{2}w_{,x}(x_a, y_a, t) + u(x_a, y_a, t) + o(u, w) \tag{12}$$

$$\Delta y_P = -\frac{h}{2}w_{,y}(x_a, y_a, t) + v(x_a, y_a, t) + o(v, w) \tag{13}$$

Similar relations hold for the lower contact point. Since Δx_P and Δy_P appear only in the argument of the functions u and w, in the geometrically linearized equations they do not make a difference, namely,

$$w(a + \Delta x_P, y, t) = w(a, y, t) + o(u, w) \tag{14}$$

2.2 Contact Forces. We now investigate the contact forces acting between one of the pins of the pad and the plate (see Fig. 4). With a pad formed by infinitely many distributed pins, these forces will be substituted by stresses. The normal force is given by

$$N_P = -N_{\bar{P}} = N_P \boldsymbol{e}_\nabla|_P$$

and the friction force is

$$\boldsymbol{R}_P = -\boldsymbol{R}_{\bar{P}} = R_P \frac{\boldsymbol{v}_{\bar{P}} - \boldsymbol{v}_P}{|\boldsymbol{v}_{\bar{P}} - \boldsymbol{v}_P|}$$

which means that its direction is opposite to the relative velocity between the pin and the contact point on the plate. Using Coulomb's law of friction

$$R_P = \mu N_P \tag{15}$$

and the force balance at the pin in $\boldsymbol{e}_z$-direction

$$(\boldsymbol{N}_{\bar{P}} + \boldsymbol{R}_{\bar{P}}) \cdot \boldsymbol{e}_z + N_0 - k(z_{\bar{P}} + h/2) = 0 \tag{16}$$

makes it possible to calculate $\boldsymbol{N}_{\bar{P}}$ and $\boldsymbol{R}_{\bar{P}}$.

The resulting contact forces can be obtained by integrating over all pins, i.e., the area B of material points in contact with the pins (see Fig. 1). Since the segments normal to the neutral plane stay rigid, according to the kinematical assumptions, loads on the surface of the plate can be replaced with an equivalent force

$$\boldsymbol{F} = F_x \boldsymbol{e}_x + F_y \boldsymbol{e}_y + F_z \boldsymbol{e}_z \tag{17}$$

and a torque

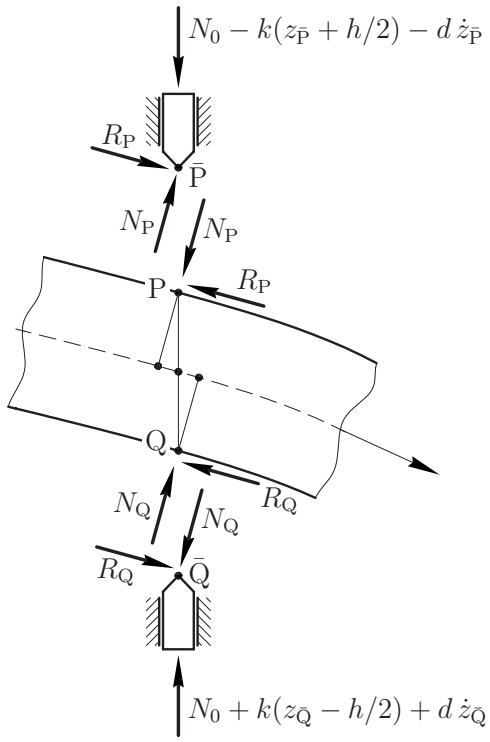

Fig. 4 Contact forces

$$\boldsymbol{T} = T_x \boldsymbol{e}_x + T_y \boldsymbol{e}_y \tag{18}$$

both acting on the neutral plane of the plate.

3 Boundary Value Problem for the Rotating Plate With Pads

3.1 Principle of Virtual Work. In Kirchhoff plate theory, the inertia of the plate is assumed to be concentrated in the neutral plane of the plate. Hence the principle of virtual work can be stated as

$$\int_V \left(\rho \frac{\mathrm{d}^2}{\mathrm{d}t^2}\boldsymbol{p}_M \cdot \delta\boldsymbol{p}_M + \sigma_{xx}\delta e_{xx} + \ \ldots\ + \sigma_{xz}\delta e_{xz}\right)\mathrm{d}V$$

$$= \int_A (\boldsymbol{F} \cdot \delta\boldsymbol{p}_M + T_x \delta w_{,y} - T_y \delta w_{,x})\mathrm{d}A \tag{19}$$

where A is the area of the surface of the plate, see Fig. 1. The terms occurring in Eq. (19) will be discussed in more detail below. The acceleration vector can be calculated from Eq. (2) by simple differentiation, noting that $\dot{x} = -\Omega y$ and $\dot{y} = \Omega x$, due to the rotation of the plate. Substituting the displacement vector (6) into the well known strain-displacement relations one obtains the strains e_{ij}. To keep expressions simple we first work with e_{ij} linearized with respect to u, v, and w. The stresses in Eq. (19) are calculated from the stress-strain relations for linear isotropic material with the plane stress assumption $\sigma_{zz} = 0$.

3.2 Derivation of a Boundary Value Problem. In order to derive the equations of motion from Eq. (19) we have to apply a variant of Gauß theorem

$$\int_V f\delta w_{,x}\mathrm{d}V = -\int_V f_{,x}\delta w \mathrm{d}V + \int_S f\delta w n_x \mathrm{d}S \tag{20}$$

several times, where n_x denotes the x-measure number of the normal vector $\boldsymbol{n}$ on S. Similar relations hold for the y- and the

z-direction. Carrying out the variations in Eq. (19) we arrive at expressions

$$\int_V f_x \delta u \mathrm{d}V + \int_S (\boldsymbol{V}^u \cdot \boldsymbol{n}) \delta u \mathrm{d}S + \int_S (\boldsymbol{M}_x^u \cdot \boldsymbol{n}) \delta u_{,x} \mathrm{d}S + \int_S (\boldsymbol{M}_y^u \cdot \boldsymbol{n}) \delta u_{,y} \mathrm{d}S + \int_V f_y \delta v \mathrm{d}V + \int_S (\boldsymbol{V}^v \cdot \boldsymbol{n}) \delta v \mathrm{d}S + \int_S (\boldsymbol{M}_x^v \cdot \boldsymbol{n}) \delta v_{,x} \mathrm{d}S + \int_S (\boldsymbol{M}_y^v \cdot \boldsymbol{n}) \delta v_{,y} \mathrm{d}S + \int_V f_z \delta w \mathrm{d}V + \int_S (\boldsymbol{V}^w \cdot \boldsymbol{n}) \delta w \mathrm{d}S + \int_S (\boldsymbol{M}_x^w \cdot \boldsymbol{n}) \delta w_{,x} \mathrm{d}S + \int_S (\boldsymbol{M}_y^w \cdot \boldsymbol{n}) \delta w_{,y} \mathrm{d}S = 0 \tag{21}$$

from which the boundary value problems for u, v, and w follow by applying the main theorem of variational calculus. It is interesting to note that the boundary value problem is by no means unique. This can be easily seen by noting that terms of the form

$$\int_V f \delta w_{,xy} \mathrm{d}V \tag{22}$$

occur. Depending on whether integration by parts is performed first for x or y, different boundary conditions arise. In fact, there are infinitely many possible boundary value problems that can be derived from Eq. (19). In order to preserve symmetries of the problem, we will treat terms of the form (22) in the following way:

$$\begin{aligned}\int_V f \delta w_{,xy} \mathrm{d}V &= \frac{1}{2}\int_V f \delta w_{,xy} \mathrm{d}V + \frac{1}{2}\int_V f \delta w_{,xy} \mathrm{d}V \\ &= \frac{1}{2}\left(- \int_V f_{,x} \delta w_{,y} \mathrm{d}V + \int_S f \delta w_{,y} n_x \mathrm{d}S \right) \\ &\quad + \frac{1}{2}\left(- \int_V f_{,y} \delta w_{,x} \mathrm{d}V + \int_S f \delta w_{,x} n_y \mathrm{d}S \right)\end{aligned} \tag{23}$$

where a second integration by parts yields

$$\begin{aligned}\int_V f \delta w_{,xy} \mathrm{d}V &= \frac{1}{2}\left(\int_V f_{,xy} \delta w \mathrm{d}V - \int_S f_{,x} \delta w n_y \mathrm{d}S + \int_S f \delta w_{,y} n_x \mathrm{d}S \right) \\ &\quad + \frac{1}{2}\left(\int_V f_{,yx} \delta w \mathrm{d}V - \int_S f_{,y} \delta w n_x \mathrm{d}S + \int_S f \delta w_{,x} n_y \mathrm{d}S \right)\end{aligned} \tag{24}$$

Choosing this symmetric approach and using the common abbreviation $D = Eh^3/12(1-\nu^2)$, the equations of motion follow as

$$\rho h u_{,tt} + 2\rho h \Omega (x u_{,ty} - y u_{,tx}) - \frac{6D}{h^2}((1-\nu)u_{,yy} + (1+\nu)v_{,xy} + 2u_{,xx}) - \rho h \Omega^2 (x - x^2 u_{,yy} + x u_{,x} + 2xy u_{,xy} + y u_{,y} - y^2 u_{,xx}) = F_x \tag{25a}$$

$$\rho h v_{,tt} + 2\rho h \Omega (x u_{,ty} - y v_{,tx}) - \frac{6D}{h^2}(1+\nu)(u_{,xy} + (1-\nu)v_{,xx} + 2v_{,yy}) - \rho h \Omega^2 (y - y^2 v_{,xx} + y v_{,y} + 2xy v_{,xy} + y u_{,y} - x^2 v_{,yy} + x v_{,x}) = F_y \tag{25b}$$

$$\rho h w_{,tt} + 2\rho h \Omega (x w_{,ty} - y w_{,tx}) + D(w_{,xxxx} + 2w_{,xxyy} + w_{,yyyy}) - \rho h \Omega^2 (y w_{,y} - x^2 w_{,yy} + x w_{,x} + 2xy w_{,xy} - y^2 w_{,xx}) = F_z - T_{x,y} + T_{y,x} \tag{26}$$

with boundary conditions following from

$$\delta u_S \int_{-h/2}^{h/2} (\sigma_{xx} n_x + \sigma_{xy} n_y) \mathrm{d}z = \delta u_S \left(\frac{12D}{h^2}(u_{,x} + \nu v_{,y}) n_x + \frac{6D(1-\nu)}{h^2}(u_{,y} + v_{,x}) n_y \right) = 0 \tag{27a}$$

$$\delta v_S \int_{-h/2}^{h/2} (\sigma_{xy} n_x + \sigma_{yy} n_y) \mathrm{d}z = \delta v_S \left(\frac{6D(1-\nu)}{h^2}(u_{,y} + v_{,x}) n_x + \frac{12D}{h^2}(\nu u_{,x} + v_{,y}) n_y \right) = 0 \tag{27b}$$

and

$$\begin{aligned}\delta w_S \int_{-h/2}^{h/2} &\left(\left(\frac{1}{h} T_y + z\sigma_{xy,y} + z\sigma_{xx,x} \right) n_x \right. \\ &\left. + \left(-\frac{1}{h} T_x + z\sigma_{yy,y} + z\sigma_{xy,x} \right) n_y \right) \mathrm{d}z \\ &= [D(w_{,xyy} + w_{,xxx}) - T_y] n_x + [D(w_{,yyy} + w_{,xxy}) + T_x] n_y = 0\end{aligned} \tag{28a}$$

$$\delta w_{S,x} \int_{-h/2}^{h/2} (z\sigma_{xx} n_x + z\sigma_{xy} n_y) \mathrm{d}z + \delta w_{S,y} \int_{-h/2}^{h/2} (z\sigma_{xy} n_x + z\sigma_{yy} n_y) \mathrm{d}z = \delta w_{S,x}(w_{,xx} + \nu w_{,yy}) n_x + \delta w_{S,y}(w_{,yy} + \nu w_{,xx}) n_y = 0 \tag{28b}$$

By inspection of the boundary value problems (26) and (28) of the plate (out-of-plane) and the boundary value problems (25) and (27) of the disk (in-plane) it can be seen that the coupling of the plate and disk equations depends on F_x, F_y, F_z and T_x, T_y only, when using the linear deformation gradient. In the linear case for the pointwise elastic model with no in-plane degree of freedom of the pad we have

$$F_i = F_i(u, u_{,j}, u_{,t}, u_{,jt}, v, v_{,j}, v_{,t}, v_{,jt}), \quad i,j \in \{x,y\} \tag{29a}$$

$$F_z = F_z(w, w_{,j}, w_{,t}, w_{,jt}), \quad j \in \{x,y\} \tag{29b}$$

$$T_i = T_i(w, w_{,j}, w_{,ij}, w_{,t}, w_{,jt}), \quad i,j \in \{x,y\} \tag{29c}$$

and therefore the plate and disk equations decouple. If second order terms are considered in the deformation gradient, we obtain the strain-displacement relations

$$e_{xx} = u_{,x} - z w_{,xx} + \tfrac{1}{2}(u_{,x}^2 + v_{,x}^2 + w_{,x}^2 + z^2 w_{,x,y} + z^2 w_{,xx}^2) + z w_{,x} u_{,xx} + z w_{,y} v_{,xx} \tag{30a}$$

$$e_{yy} = v_{,y} - z w_{,yy} + \tfrac{1}{2}(u_{,y}^2 + v_{,y}^2 + w_{,y}^2 + z^2 w_{,x,y} + z^2 w_{,yy}^2) + z w_{,x} u_{,yy} + z w_{,y} v_{,yy} \tag{30b}$$

$$e_{zz} = 0 \tag{30c}$$

$$e_{xy} = \tfrac{1}{2} u_{,y} + \tfrac{1}{2} v_{,x} - z w_{,xy} + \tfrac{1}{2}(u_{,y} u_{,x} + v_{,y} v_{,x} + w_{,y} w_{,x} + z^2 (w_{,yy} w_{,xy} + w_{,xy} w_{,xx})) + z(w_{,x} u_{,xy} + w_{,y} v_{,xy}) \tag{30d,e}$$

$$e_{yz} = 0 \tag{30f}$$

$$e_{xz} = 0 \tag{30g}$$

and it is clear that the quadratic terms containing w, u, and v will yield a coupling of the disk and plate equations after taking the variation of e_{ij} [3]. We note, however, that due to the integration of the equations over z the coupling occurs only through nonlinear terms. A second fact to be noted is that, when linearizing the equations about a prestressed configuration, i.e., $\sigma_{ij}=\sigma_{ij}^0+\Delta\sigma_{ij}$, the prestress terms only enter the equations of motion if the nonlinear deformation gradient is used. With the linear deformation gradient terms of the form $\sigma_{ij}^0\delta e_{ij}$ vanish in the process of integrating by parts. This is why the effect of centrifugal stiffening [8] does not appear even when the equations of motion are linearized about a prestressed configuration. Since we are particularly interested in small deformations of the plate we continue working with the linearized strain relations and discuss the influence of centrifugal stiffening in Sec. 4.4.

3.3 Transformation to Polar Coordinates. We will now transform our equations into polar coordinates, i.e., we will express the functions u, v, and w and the components of the normal vector $\boldsymbol{n}$ in polar coordinates. The function $w(x,y,t)$ and its derivatives can be written in polar coordinates using

$$\frac{\partial^{a+b}}{\partial x^a\,\partial y^b}w(x,y,t) = \frac{\partial^{a+b}}{\partial x^a\,\partial y^b}\tilde{w}(r(x,y),\varphi(x,y),t) \tag{31}$$

and noting that $r(x,y)=\sqrt{x^2+y^2}$ and $\varphi(x,y)=\arctan(y/x)$. After carrying out the differentiations we set $x=r\cos\varphi$ and $y=r\sin\varphi$. For u and v we proceed similarly by writing

$$u(x,y,t) = \tilde{u}(r,\varphi,t)\cos\varphi - \tilde{v}(r,\varphi,t)\sin\varphi \tag{32a}$$

$$v(x,y,t) = \tilde{v}(r,\varphi,t)\cos\varphi + \tilde{u}(r,\varphi,t)\sin\varphi \tag{32b}$$

which means that we define a new displacement vector for points on the neutral plane

$$\boldsymbol{u}_M = \tilde{u}(r,\varphi,t)\boldsymbol{e}_r + \tilde{v}(r,\varphi,t)\boldsymbol{e}_\varphi + \tilde{w}(r,\varphi,t)\boldsymbol{e}_z \tag{33}$$

In the following we omit the tilde in $\tilde{u}(r,\varphi,t)$, $\tilde{v}(r,\varphi,t)$, and $\tilde{w}(r,\varphi,t)$. There should be no confusion between $u(x,y,t)$, $v(x,y,t)$, $w(x,y,t)$ and $\tilde{u}(r,\varphi,t)$, $\tilde{v}(r,\varphi,t)$, $\tilde{w}(r,\varphi,t)$ since they can be distinguished by their arguments and by the context.

3.3.1 Contact Forces. The contact forces and torques contain contributions of the upper and the lower pad, which read

$$F_r^P = \kappa(r,\varphi)\left(-N_0 w_{,r} - h\mu N_0\left(\frac{w_{,tr}}{2r\Omega} + \frac{w_{,r\varphi}}{2r} - \frac{w_{,\varphi}}{2r^2}\right) + \mu N_0\frac{\Omega(v-u_{,\varphi})-u_{,t}}{r\Omega}\right) \tag{34a}$$

$$F_r^Q = \kappa(r,\varphi)\left(N_0 w_{,r} + h\mu N_0\left(\frac{w_{,tr}}{2r\Omega} + \frac{w_{,r\varphi}}{2r} - \frac{w_{,\varphi}}{2r^2}\right) + \mu N_0\frac{\Omega(v-u_{,\varphi})-u_{,t}}{r\Omega}\right) \tag{34b}$$

$$F_\varphi^P = \kappa(r,\varphi)\left(-\mu N_0 + k\mu w - \frac{N_0}{r}(1+\mu^2)w_{,\varphi}\right) \tag{34c}$$

$$F_\varphi^Q = \kappa(r,\varphi)\left(-\mu N_0 - k\mu w + \frac{N_0}{r}(1+\mu^2)w_{,\varphi}\right) \tag{34d}$$

$$F_z^P = \kappa(r,\varphi)(N_0 - kw) \tag{34e}$$

$$F_z^Q = \kappa(r,\varphi)(-N_0 - kw) \tag{34f}$$

and the contact torques are obtained from

$$\boldsymbol{T}^P = \frac{h}{2}\boldsymbol{e}_\nabla \times (F_r^P\boldsymbol{e}_r + F_\varphi^P\boldsymbol{e}_\varphi + F_z^P\boldsymbol{e}_z) \tag{35a}$$

$$\boldsymbol{T}^Q = -\frac{h}{2}\boldsymbol{e}_\nabla \times (F_r^Q\boldsymbol{e}_r + F_\varphi^Q\boldsymbol{e}_\varphi + F_z^Q\boldsymbol{e}_z) \tag{35b}$$

where $\kappa(r,\varphi)$ is a weight function describing the area of the pads. It can be chosen to be a continuous function or, for example, as $\kappa(r,\varphi)=1$ if $(r,\varphi)\in B$, i.e., if (r,φ) are in the domain of the pad (denoted by B to be distinguished from the whole area of the plate surface denoted earlier by A) and $\kappa(r,\varphi)=0$ otherwise. In principle it would be possible to assume that all pad parameters depend on r and φ, to introduce more generality into the model. No realistic data are, however, currently available on such distributions from experiments, and for the sake of simplicity we do not proceed further in that direction. In the linear case the normal vector reads

$$\boldsymbol{e}_\nabla = -w_{,r}\boldsymbol{e}_r - \frac{w_{,\varphi}}{r}\boldsymbol{e}_\varphi + \boldsymbol{e}_z \tag{36}$$

and it follows that

$$F_r = F_r^P + F_r^Q = \kappa(r,\varphi)2\mu N_0\frac{\Omega(v-u_{,\varphi})-u_{,t}}{r\Omega} \tag{37a}$$

$$F_\varphi = F_\varphi^P + F_\varphi^Q = -\kappa(r,\varphi)2\mu N_0 \tag{37b}$$

$$F_z = F_z^P + F_z^Q = -\kappa(r,\varphi)2kw \tag{37c}$$

$$T_r = T_r^P + T_r^Q = \kappa(r,\varphi)\left(hk\mu w - \frac{hN_0\mu^2 w_{,\varphi}}{r}\right) \tag{37d}$$

$$T_\varphi = T_\varphi^P + T_\varphi^Q = \kappa(r,\varphi)h^2N_0\mu\left(\frac{w_{,rt}}{2r\Omega} - \frac{w_{,\varphi}}{2r^2} + \frac{w_{,r\varphi}}{2r}\right) \tag{37e}$$

where many terms from the upper and lower pads cancel, so that the in-plane forces F_r and F_φ depend on u and v and their derivatives only, whereas F_z, T_r, and T_φ only depend on w and its derivatives. This is the justification for Eq. (29), which explains the decoupling of disk and plate equations, as discussed in Sec. 3.2. It is due to the assumption that the pads do not have a degree of freedom in the in-plane direction. The dependence of F_r and F_φ on u and v comes from the relative velocity of the contact points on the pad and the plate. If we would give the upper and the lower pad independent degrees of freedom in the in-plane direction, say, $u_{\bar{P}}$ and $v_{\bar{P}}$ for the upper pad, they would appear in the relative velocity. Therefore if the in-plane degrees of freedom of the upper and lower pads are independent, they will appear in F_r, F_φ and T_r, T_φ and thus couple the disk and plate equations. Note that in practice in-plane vibrations are possible and were detected [6]. The analysis shows that they can either be explained through nonlinear coupling of disk and plate equations or that a linear coupling can arise through in-plane degrees of freedom of the pads, which also occur in practice.

3.3.2 Plate Equations. Transforming the plate equations into polar coordinates we obtain

$$\rho h w_{,tt} + 2h\rho\Omega w_{,t\varphi} + \Omega^2\rho h w_{,\varphi\varphi} + \frac{D}{r^4}(4w_{,\varphi\varphi} + w_{,\varphi\varphi\varphi\varphi}) + \frac{D}{r^3}(w_{,r} + 2w_{,r\varphi\varphi}) + \frac{D}{r^2}(2w_{,rr\varphi\varphi} - w_{,rr}) + 2\frac{D}{r}w_{,rrr} + Dw_{,rrrr} = F_z - \frac{1}{r}T_{r,\varphi} + T_{\varphi,r} \tag{38}$$

where the transformed natural boundary operators read

$$\boldsymbol{V}^w = V_r^w\boldsymbol{e}_r + V_\varphi^w\boldsymbol{e}_\varphi \tag{39a}$$

$$V_r^w = -M_\varphi + \frac{2D}{r^3}w_{,\varphi\varphi} + \frac{D}{r^2}(w_{,r} - w_{,r\varphi\varphi}) - \frac{D}{r}w_{,rr} - Dw_{,rrr} \tag{39b}$$

$$V_\varphi^w = M_r - \frac{D}{r^3}w_{,\varphi\varphi\varphi} - \frac{D}{r^2}w_{,r\varphi} - \frac{D}{r}w_{,rr\varphi} \tag{39c}$$

and

$$\boldsymbol{M} = M_r\boldsymbol{e}_r + M_\varphi\boldsymbol{e}_\varphi \tag{39d}$$

$$M_r = -\frac{D}{r^2}(1-\nu)w_{,\varphi} + \frac{D}{r}(1-\nu)w_{,r\varphi} \tag{39e}$$

$$M_\varphi = \frac{D\nu}{r^2}w_{,\varphi\varphi} + \frac{D\nu}{r}w_{,r} + Dw_{,rr} \tag{39f}$$

For the annular plate, clamped at the inner and free at the outer radius, we obtain the geometric boundary conditions $w|_{r=r_i}=0$ and $w_{,r}|_{r=r_i}=0$, and the natural boundary conditions $V_r|_{r=r_o}=0$ and $M_r|_{r=r_o}=0$.

3.3.3 Disk Equations. The boundary value problem for the disk in polar coordinates reads

$$\rho h\begin{bmatrix}1 & 0\\ 0 & 1\end{bmatrix}\begin{bmatrix}\ddot{u}\\ \ddot{v}\end{bmatrix} + \begin{bmatrix}\kappa 2\dfrac{\mu N_0}{r\Omega} + 2\Omega\rho h\dfrac{\partial}{\partial\varphi} & -2\Omega\rho h\\ 2\Omega\rho h & 2\Omega\rho h\dfrac{\partial}{\partial\varphi}\end{bmatrix}\begin{bmatrix}\dot{u}\\ \dot{v}\end{bmatrix} + \begin{bmatrix}L_{11} & L_{12}\\ L_{21} & L_{22}\end{bmatrix}\begin{bmatrix}u\\ v\end{bmatrix} = \begin{bmatrix}\rho h\Omega^2 r\\ -\kappa 2\mu N_0\end{bmatrix} \tag{40}$$

(where as before $\kappa=\kappa(r,\varphi)$) with the linear operators

$$L_{11} = -\frac{Eh}{1-\nu^2}\left(\frac{\partial^2}{\partial r^2} + \frac{1}{r}\frac{\partial}{\partial r} - \frac{1}{r^2} + \frac{1-\nu}{2r^2}\frac{\partial^2}{\partial\varphi^2}\right) - \rho h\Omega^2\left(1 - \frac{\partial^2}{\partial\varphi^2}\right) + \kappa 2\frac{\mu N_0}{r}\frac{\partial}{\partial\varphi} \tag{41a}$$

$$L_{12} = -\frac{Eh}{1-\nu^2}\left(\frac{1+\nu}{2}\frac{1}{r}\frac{\partial^2}{\partial r\,\partial\varphi} - \frac{3-\nu}{2}\frac{1}{r^2}\frac{\partial}{\partial\varphi}\right) - 2\rho h\Omega^2\frac{\partial}{\partial\varphi} - \kappa 2\frac{\mu N_0}{r} \tag{41b}$$

$$L_{21} = -\frac{Eh}{1-\nu^2}\left(\frac{1+\nu}{2}\frac{1}{r}\frac{\partial^2}{\partial r\,\partial\varphi} + \frac{3-\nu}{2}\frac{1}{r^2}\frac{\partial}{\partial\varphi}\right) + 2\rho h\Omega^2\frac{\partial}{\partial\varphi} \tag{41c}$$

$$L_{22} = -\frac{Eh}{1-\nu^2}\left(\frac{1-\nu}{2}\left(\frac{\partial^2}{\partial r^2} + \frac{1}{r}\frac{\partial}{\partial r} - \frac{1}{r^2}\right) + \frac{1}{r^2}\frac{\partial^2}{\partial\varphi^2}\right) - \rho h\Omega^2\left(1 - \frac{\partial^2}{\partial\varphi^2}\right) \tag{41d}$$

and the natural boundary operators

$$\boldsymbol{V}^{u,v} = V_r^{u,v}\boldsymbol{e}_r + V_\varphi^{u,v}\boldsymbol{e}_\varphi \tag{42a}$$

$$V_r^u = \frac{1}{1-\nu^2}\left[u_{,r} + \nu\left(\frac{u}{r} + \frac{1}{r}v_{,\varphi}\right)\right] \tag{42b}$$

$$V_r^v = \frac{1}{2(1+\nu)}\left[\frac{1}{r}u_{,\varphi} + v_{,r} - \frac{v}{r}\right] \tag{42c}$$

$$V_\varphi^v = \frac{1}{2(1+\nu)}\left[\frac{1}{r}u_{,\varphi} + v_{,r} - \frac{v}{r}\right] \tag{42d}$$

$$V_\varphi^v = \frac{1}{1-\nu^2}\left[\frac{u}{r} + \frac{1}{r}v_{,\varphi} + \nu u_{,r}\right] \tag{42e}$$

For the annular disk clamped at the inner radius r_i and free at the outer radius r_o we have the geometric boundary conditions $u|_{r=r_i}=v|_{r=r_i}=0$ and the natural boundary conditions $V_r^u|_{r=r_o}=V_r^v|_{r=r_o}=0$. For $\mu=0$, that is, neglecting F_r and F_φ, the boundary value problem coincides with the one derived in Ref. [16]. Equations (40) and (42) form a linear inhomogeneous boundary value problem of which the solution is given by the general solution of the homogeneous boundary value problem plus a particular solution. Its stability can be studied investigating the stability of the trivial solution of the homogeneous boundary value problem.

3.4 Comparison to the Results Obtained Previously. In comparison to the results obtained in Ref. [13] using the Ritz discretization approach, two major differences shall be discussed. The first one is that in the continuous approach we use surface contact between disk and pads. The reason for this is that the Kirchhoff plate cannot deal with finite torques applied at points. A finite torque $\hat{\boldsymbol{T}}=\hat{T}_x\boldsymbol{e}_x+\hat{T}_y\boldsymbol{e}_y$ applied at a single point (x_a,y_a) of the plate appears in the principle of virtual work as a term

$$\delta W = \hat{T}_x\delta w_y(x_a,y_a,t) - \hat{T}_y\delta w_x(x_a,y_a,t) \tag{43}$$

After carrying out the variations there is no further term containing $\delta w_x(x_a,y_a,t)$ or $\delta w_y(x_a,y_a,t)$, since in δe_{ij} no term of the form $\delta w_{,xyy}$ or $\delta w_{,xxy}$ arises. Therefore one would conclude from the main theorem of variational calculus that $\hat{\boldsymbol{T}}=\boldsymbol{0}$, which is a contradiction. The Kirchhoff plate can therefore not resist finite torques applied at points. It is, however, very well able to resist finite transverse forces applied at points. Their contribution to the virtual work is

$$\delta W = \hat{F}_z\delta w(x_a,y_a,t) \tag{44}$$

Further terms containing $\delta w(x_a,y_a,t)$ arise from integration by parts of the term (22), yielding conditions for corner forces of different sections of the plate.

The second fact to be noted is that we used a strategy for linearization different from the one used in Ref. [13]. Whereas in Ref. [13] energy expressions were expanded in a Taylor series up to second order, to be sure to obtain the complete linear equations, in the boundary value problem derived in the present case only the linear contact forces appear, because a purely geometric linearization has been performed. The terms Δx_P and Δy_P therefore do not enter the equations of motion as explained in Sec. 2.1 with Eq. (14).

Another difference is that we got rid of the kinematic assumption that points on the neutral plane can only move transversely in the rotating frame, allowing for in-plane deformations of the plate. Nevertheless we again stress that this does not yield a term depending on u and v in the linearized contact forces, which would mean plate and disk equations cannot be solved independently.

Summarizing the previous results, we note that the boundary value problems of the plate and disk are decoupled as long as no in-plane motions of the pads are considered in the model. Furthermore a centrifugal stiffening cannot arise in the equations of motion when working with the linear deformation gradient. We have also recalled the well known fact from Kirchhoff theory that the plate is not capable to withstand finite torques (see, e.g., Ref. [17]).

4 Perturbation Analysis

We now interpret the terms arising from the pads as perturbations, i.e., in Eqs. (38) and (39) and Eqs. (40) and (42) we replace k with γk, and N_0 with δN_0. For the following calculations we introduce the dimensionless time $\bar{t}=t/r_o\sqrt{E/\rho}$ and the radius $\bar{r}=r/r_o$ yielding the dimensionless parameters

$$\bar{\Omega} = \Omega r_o \sqrt{\frac{\rho}{E}}, \quad \bar{r}_i = \frac{r_i}{r_o}, \quad \bar{r}_{pi} = \frac{r_{pi}}{r_o}, \quad \bar{r}_{po} = \frac{r_{po}}{r_o} \tag{45}$$

$$\bar{h} = \frac{h}{r_o}, \quad \bar{k} = k\frac{r_o}{E}, \quad \bar{N}_0 = \frac{N_0}{E}, \quad \bar{D} = \frac{\bar{h}^3}{12(1-\nu^2)} \tag{46}$$

To simplify notation, in the following the bars are omitted and derivatives are to be understood as derivatives with respect to the dimensionless variables. It will be shown in the sequel that by separating time from the equations, the boundary value problems for the plate and the disk can be written in the form

$$\boldsymbol{L}(\boldsymbol{w}) = \boldsymbol{L}^0(\boldsymbol{w}) + \gamma \boldsymbol{L}^{1\gamma}(\boldsymbol{w}) + \delta \boldsymbol{L}^{1\delta}(\boldsymbol{w}) = 0 \tag{47a}$$

$$\boldsymbol{U}_i(\boldsymbol{w}) = \boldsymbol{U}_i^0(\boldsymbol{w}) = 0 \tag{47b}$$

where we denote by $\boldsymbol{L}$ the operator matrix corresponding to the eigenvalue problem and $\boldsymbol{U}_i$ are operator matrices corresponding to the boundary conditions. In the plate problem we set $w(r,\varphi,t) = \bar{w}(r,\varphi)e^{\lambda t}$, where we again skip the bar for notational simplicity. The boundary value problem can be stated as

$$L^0(w) = \lambda^2 w + 2\lambda\Omega w_{,\varphi} + \Omega^2 w_{,\varphi\varphi} + \frac{D}{r^4}(4w_{,\varphi\varphi} + w_{,\varphi\varphi\varphi\varphi}) + \frac{D}{r^3}(w_{,r} + 2w_{,r\varphi\varphi}) + \frac{D}{r^2}(2w_{,rr\varphi\varphi} - w_{,rr}) + 2\frac{D}{r}w_{,rrr} + Dw_{,rrrr} \tag{48a}$$

$$L^{1\gamma}(w) = \kappa(r,\varphi)2kw - \left(\kappa(r,\varphi)\frac{hk\mu w}{r}\right)_{,\varphi} \tag{48b}$$

$$L^{1\delta}(w) = -\left(\kappa(r,\varphi)h^2 N_0 \mu\left(\lambda\frac{w_{,rt}}{2r\Omega} - \frac{w_{,\varphi}}{2r^2} + \frac{w_{,r\varphi}}{2r}\right)\right)_{,r} \tag{48c}$$

with boundary conditions

$$U_1 = w(r_i,\varphi,t) = 0, \quad U_2 = w_{,r}(r_i,\varphi,t) = 0 \tag{49}$$

$$U_3 = V_r^w|_{r=r_o} = 0, \quad U_4 = M_r|_{r=r_o} = 0 \tag{50}$$

where the operators for the differential equation and the boundary conditions act on the scalar function w and are therefore not represented by bold characters. In case $\kappa(r,\varphi)$ is chosen as a discontinuous function, we note that $L^{1\gamma}$ and $L^{1\delta}$ contain transition terms. In the perturbation formulas derived later, they can easily be eliminated by integration by parts. There are no perturbations in the boundary condition (47*b*); the boundary conditions of the perturbed problem therefore coincide with those of the unperturbed problem.

For the disk we perform the ansatz of separation of variables

$$\begin{bmatrix} u(r,\varphi,t) \\ v(r,\varphi,t) \end{bmatrix} = \begin{bmatrix} \bar{u}(r,\varphi) \\ \bar{v}(r,\varphi) \end{bmatrix} e^{\lambda t} = \boldsymbol{w} e^{\lambda t} \tag{51}$$

for simplicity skipping the bar for u and v; this yields the operators

$$\boldsymbol{L}^0(\boldsymbol{w}) = \left[\lambda^2\begin{bmatrix} 1 & 0 \\ 0 & 1 \end{bmatrix} + \lambda\begin{bmatrix} 2\Omega\dfrac{\partial}{\partial\varphi} & -2\Omega \\ 2\Omega & 2\Omega\dfrac{\partial}{\partial\varphi} \end{bmatrix} + \begin{bmatrix} L_{11}^0 & L_{12}^0 \\ L_{21}^0 & L_{22}^0 \end{bmatrix}\right]\begin{bmatrix} u \\ v \end{bmatrix} \tag{52a}$$

$$\boldsymbol{L}^{1\gamma}(\boldsymbol{w}) = \boldsymbol{0} \tag{52b}$$

$$\boldsymbol{L}^{1\delta}(\boldsymbol{w}) = \kappa(r,\varphi)\left[\lambda\begin{bmatrix} \dfrac{2\mu N_0}{r\Omega} & 0 \\ 0 & 0 \end{bmatrix} + \begin{bmatrix} \dfrac{2\mu N_0}{r} & -\dfrac{2\mu N_0}{r} \\ 0 & 0 \end{bmatrix}\right]\begin{bmatrix} u \\ v \end{bmatrix} \tag{52c}$$

where

$$L_{11}^0 = -\frac{1}{1-\nu^2}\left(\frac{\partial^2}{\partial r^2} + \frac{1}{r}\frac{\partial}{\partial r} - \frac{1}{r^2} + \frac{1-\nu}{2r^2}\frac{\partial^2}{\partial\varphi^2}\right) - \Omega^2\left(1 - \frac{\partial^2}{\partial\varphi^2}\right) \tag{53a}$$

$$L_{12}^0 = -\frac{1}{1-\nu^2}\left(\frac{1+\nu}{2}\frac{1}{r}\frac{\partial^2}{\partial r\,\partial\varphi} - \frac{3-\nu}{2}\frac{1}{r^2}\frac{\partial}{\partial\varphi}\right) - 2\Omega^2\frac{\partial}{\partial\varphi} \tag{53b}$$

$$L_{21}^0 = -\frac{1}{1-\nu^2}\left(\frac{1+\nu}{2}\frac{1}{r}\frac{\partial^2}{\partial r\,\partial\varphi} + \frac{3-\nu}{2}\frac{1}{r^2}\frac{\partial}{\partial\varphi}\right) + 2\Omega^2\frac{\partial}{\partial\varphi} \tag{53c}$$

$$L_{22}^0 = -\frac{1}{1-\nu^2}\left(\frac{1-\nu}{2}\left(\frac{\partial^2}{\partial r^2} + \frac{1}{r}\frac{\partial}{\partial r} - \frac{1}{r^2}\right) + \frac{1}{r^2}\frac{\partial^2}{\partial\varphi^2}\right) - \Omega^2\left(1 - \frac{\partial^2}{\partial\varphi^2}\right) \tag{53d}$$

and the natural boundary conditions read

$$\boldsymbol{U}_1(\boldsymbol{w}) = \begin{bmatrix} 1 & 0 \\ 0 & 1 \end{bmatrix}\begin{bmatrix} u(r,t) \\ v(r,t) \end{bmatrix}\Bigg|_{r=r_i} = \boldsymbol{0} \tag{54a}$$

$$\boldsymbol{U}_2(\boldsymbol{w}) = \begin{bmatrix} \dfrac{\partial}{\partial r} + \nu\dfrac{1}{r} & \dfrac{1}{r}\dfrac{\partial}{\partial\varphi} \\ \dfrac{1}{r}\dfrac{\partial}{\partial\varphi} & \dfrac{\partial}{\partial r} - \dfrac{1}{r} \end{bmatrix}\begin{bmatrix} u(r,t) \\ v(r,t) \end{bmatrix}\Bigg|_{r=r_o} = \boldsymbol{0} \tag{54b}$$

We assume that the parameters δ and γ are smooth functions of a parameter ε. This corresponds to a variation along a smooth curve parametrized by ε in the parameter space [14,15]. It is possible to expand $\delta(\varepsilon)$ and $\gamma(\varepsilon)$ around $\varepsilon=0$ assuming that $\delta(0)=\gamma(0)=0$, for example,

$$\gamma(\varepsilon) = \gamma_{,\varepsilon}(0)\varepsilon + \cdots = \gamma_1\varepsilon + \cdots \tag{55}$$

$$\delta(\varepsilon) = \delta_{,\varepsilon}(0)\varepsilon + \cdots = \delta_1\varepsilon + \cdots \tag{56}$$

Assuming this kind of perturbation we write the perturbed boundary value problem up to first order in ε as

$$\boldsymbol{L}(\boldsymbol{w}) + \varepsilon\boldsymbol{L}^{1\varepsilon}(w) = 0 \tag{57}$$

$$\boldsymbol{U}_i(\boldsymbol{w}) = 0 \tag{58}$$

where $\boldsymbol{L}^{1\varepsilon} = \gamma_1\boldsymbol{L}^{1\gamma} + \delta_1\boldsymbol{L}^{1\delta}$.

According to Refs. [18,15,14], for a simple eigenvalue λ_0 and the corresponding eigenfunction $\mathbf{u}$, we set

$$\boldsymbol{w} = \boldsymbol{u} + \varepsilon\boldsymbol{w}_1^\varepsilon + \cdots \tag{59}$$

$$\lambda = \lambda_0 + \varepsilon\lambda_1^\varepsilon + \cdots = \lambda_0 + \varepsilon(\gamma_1\lambda_1^\gamma + \delta_1\lambda_1^\delta) + \cdots \tag{60}$$

Substitution into Eq. (57), taking the scalar product with the eigenfunction $\boldsymbol{v}$ of the adjoint of the unperturbed problem, and collecting the terms linear in ε yield

$$\lambda_1^\varepsilon = -\frac{\langle\boldsymbol{L}^{1\varepsilon}(\boldsymbol{u}),\boldsymbol{v}\rangle}{\left\langle\dfrac{\partial\boldsymbol{L}^0}{\partial\lambda}(\boldsymbol{u}),\boldsymbol{v}\right\rangle} \tag{61}$$

where $\langle\boldsymbol{u},\boldsymbol{v}\rangle = \int_A \boldsymbol{v}^*\boldsymbol{u}\,dA$, the asterisk denotes complex conjugate transpose.

For a semisimple eigenvalue λ_0 of the unperturbed problem, a double eigenvalue with two linearly independent (matrix) eigenfunctions, with corresponding eigenfunctions $\boldsymbol{u}_1$ and $\boldsymbol{u}_2$ substituting $\boldsymbol{u}=\alpha_1\boldsymbol{u}_1+\alpha_2\boldsymbol{u}_2$ in Eq. (59) and collecting terms linear in ε yields [15]

$$\boldsymbol{L}^{1\varepsilon}(\alpha_1\boldsymbol{u}_1+\alpha_2\boldsymbol{u}_2)+\lambda_1^{\varepsilon}\frac{\partial\boldsymbol{L}^0}{\partial\lambda_0}(\alpha_1\boldsymbol{u}_1+\alpha_2\boldsymbol{u}_2)=\boldsymbol{0} \tag{62}$$

The scalar product with the corresponding two eigenfunctions $\boldsymbol{v}_1$ and $\boldsymbol{v}_2$ of the adjoint of the unperturbed problem yields

$$\begin{bmatrix} \langle \boldsymbol{L}^{1\varepsilon}(\boldsymbol{u}_1),\boldsymbol{v}_1\rangle+\lambda_1^{\varepsilon}\left\langle\frac{\partial\boldsymbol{L}^0}{\partial\lambda}(\boldsymbol{u}_1),\boldsymbol{v}_1\right\rangle & \langle \boldsymbol{L}^{1\varepsilon}(\boldsymbol{u}_1),\boldsymbol{v}_2\rangle+\lambda_1^{\varepsilon}\left\langle\frac{\partial\boldsymbol{L}^0}{\partial\lambda}(\boldsymbol{u}_1),\boldsymbol{v}_2\right\rangle \\ \langle \boldsymbol{L}^{1\varepsilon}(\boldsymbol{u}_2),\boldsymbol{v}_1\rangle+\lambda_1^{\varepsilon}\left\langle\frac{\partial\boldsymbol{L}^0}{\partial\lambda}(\boldsymbol{u}_2),\boldsymbol{v}_1\right\rangle & \langle \boldsymbol{L}^{1\varepsilon}(\boldsymbol{u}_2),\boldsymbol{v}_2\rangle+\lambda_1^{\varepsilon}\left\langle\frac{\partial\boldsymbol{L}^0}{\partial\lambda}(\boldsymbol{u}_2),\boldsymbol{v}_2\right\rangle \end{bmatrix}\begin{bmatrix}\alpha_1\\ \alpha_2\end{bmatrix}=\boldsymbol{0} \tag{63}$$

For nontrivial solutions in α_1 and α_2, the determinant of the matrix has to vanish, which yields λ_1^{ε}. An analogous formula describing the splitting of a semisimple eigenvalue of multiplicity r

$$\det\left[\langle \boldsymbol{L}^{1\varepsilon}\boldsymbol{u}_k,\boldsymbol{v}_j\rangle+\lambda_1^{\varepsilon}\left\langle\frac{\partial\boldsymbol{L}^0}{\partial\lambda}\boldsymbol{u}_k,\boldsymbol{v}_j\right\rangle\right]=0,\quad j,k=1,\ldots,r \tag{64}$$

generalizes the result derived for scalar differential operators in Ref. [15] to the case of operator matrices. We note that the approach based on the perturbation theory of multiple eigenvalues [19] differs from that used in Ref. [20] and allows one to study the phenomena of veering and overlapping of eigenvalue branches with the use of operator derivatives and eigenvectors of a multiple eigenvalue calculated only for the values of parameters corresponding to coalescence of eigenvalues.

4.1 Spectrum of the Unperturbed Problem

4.1.1 Plate. We investigate the unperturbed boundary eigenvalue problem of the plate

$$L^0(w)=0 \tag{65}$$

$$U_i(w)=0,\quad i=1,\ldots,4 \tag{66}$$

and expand w in terms of the eigenfunctions of the corresponding nonrotating plate, that is, $\Omega=0$,

$$w(r,\varphi,t)=\sum_{i=0}^{\infty}\left(W_i^c(r,\varphi)q_i^c(t)+W_i^s(r,\varphi)q_i^s(t)\right) \tag{67}$$

The boundary eigenvalue problem obtained after separation of time for the nonrotating annular plate in dimensionless form reads

$$\nabla^4W(r,\varphi)=\frac{h}{D}\omega_{mn}^2W(r,\varphi) \tag{68}$$

$$W(r_i,\varphi)=0,\quad W_{,r}(r_i,\varphi)=0 \tag{69}$$

$$M_r(r_o,\varphi)=0,\quad V_r(r_o,\varphi)=0 \tag{70}$$

where V_r and M_r are given in Eqs. (39*b*) and (39*e*), respectively.

According to Ref. [21], the eigenfunctions are

$$W_i^c(r,\varphi)=R_{mn}(r)\cos m\varphi,\quad m=0,\ldots,\infty,\quad n=1,\ldots,\infty$$

$$W_i^s(r,\varphi)=R_{mn}(r)\sin m\varphi,\quad m=\infty,\ldots,0,\quad n=\infty,\ldots,1$$

where the $R_{mn}(r)=C_1I(\beta_{mn}r)+C_2J(\beta_{mn}r)+C_3Y(\beta_{mn}r)+C_4K(\beta_{mn}r)$ are linear combinations of Bessel and modified Bessel functions, and the constants $C_1,\ldots,C_4$ are determined from the linear equation after substitution of the ansatz into the boundary conditions (69) and (70). The quantities $\beta_{mn}=\sqrt[4]{(h/D)\omega_{mn}^2}$ are the roots of the characteristic equation resulting from equating the determinant of the matrix of the linear system to zero. The numbers (m,n) denote the number of nodal diameters and nodal circles of the plate. Since the plate is clamped at the inner radius, numeration of nodes n starts from $n=1$. The functions $W_i^c(r,\varphi)$ corresponding to $m=0$ are umbrella modes of the plate. The eigenfunctions for the nonrotating annular plate are known to form a complete orthogonal base for the problem of the rotating plate. We now project the problem of the rotating plate onto the eigenfunctions of the nonrotating plate, i.e., we write

$$\int_A L^0(w)W_j^c\mathrm{d}A=\int_A L^0\left(\sum_{i=0}^{\infty}\left(W_i^cq_i^c+W_i^sq_i^s\right)\right)W_i^c\mathrm{d}A=0 \tag{71}$$

$$\int_A L^0(w)W_j^s\mathrm{d}A=\int_A L^0\left(\sum_{i=0}^{\infty}\left(W_i^cq_i^c+W_i^sq_i^s\right)\right)W_i^s\mathrm{d}A=0 \tag{72}$$

Equations (71) and (72) form an infinite dimensional matrix equation of the type

$$(\boldsymbol{M}\lambda^2+\boldsymbol{G}\lambda+\boldsymbol{K})\boldsymbol{q}=\boldsymbol{0},\quad \boldsymbol{q}=[q_1^c,\ldots,q_\infty^c,q_\infty^s,\ldots,q_1^s]^T$$

Using this and the orthogonality relations for the trigonometric functions sin and cos and the orthogonality of the eigenfunctions of the nonrotating plate we find that the matrices of the unperturbed problem read

$$\boldsymbol{M}=\mathrm{diag}(M_{mn}) \tag{73}$$

$$\boldsymbol{G}=\mathrm{antidiag}(2mM_{mn}\Omega,-2mM_{mn}\Omega) \tag{74}$$

$$\boldsymbol{K}=\mathrm{diag}(\omega_{mn}^2M_{mn}-m^2M_{mn}\Omega^2) \tag{75}$$

where $M_{mn}=h\pi\int_{r_i}^{r_o}R_{mn}^2(r)r\mathrm{d}r$. Consequently, the equations of motion of the unperturbed problem decouple into infinitely many pairs of two coupled equations of the form

$$\begin{bmatrix}1&0\\0&1\end{bmatrix}\ddot{\boldsymbol{q}}+\begin{bmatrix}0&-2m\Omega\\2m\Omega&0\end{bmatrix}\dot{\boldsymbol{q}}+\begin{bmatrix}\omega_{mn}^2-m^2\Omega^2&0\\0&\omega_{mn}^2-m^2\Omega^2\end{bmatrix},$$

$$\boldsymbol{q}=0,\quad m>0 \tag{76}$$

where we divided it by M_{mn}. The spectrum of the unperturbed problem, namely, the eigenvalues of Eq. (76), can be calculated analytically as

$$\lambda^{1\pm}=\pm i(\omega_{mn}+m\Omega) \tag{77a}$$

$$\lambda^{2\pm}=\pm i(\omega_{mn}-m\Omega) \tag{77b}$$

and form the geometric structure called a spectral mesh in Ref. [22] depicted in Fig. 5 for the dimensionless parameters

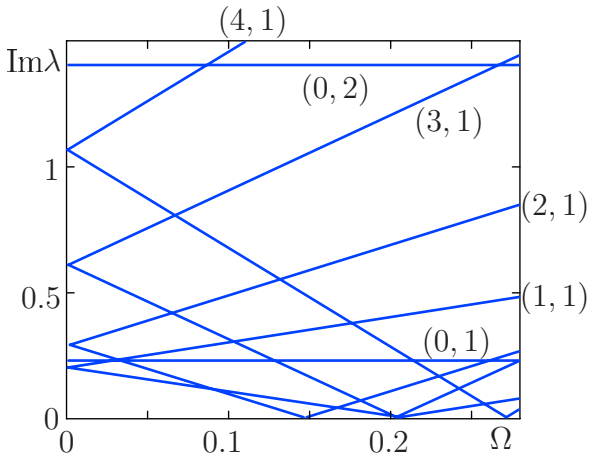

Fig. 5 Spectrum of the out-of-plane vibrations of the unperturbed problem (plate) for r_i=0.154 (spectral mesh)

$$h = 0.1605, \quad D = 3.7858 \times 10^{-4}, \quad r_i = 0.154, \quad \nu = 0.3 \tag{78}$$

which are based on the parameters for a disk brake used in Ref. [13]. They correspond to a brake rotor represented by an equivalent Kirchhoff plate with r_o=0.162 m, E=4.16×10^{10} N/m, and ρ=4846 kg/m^3. These parameters were identified in Ref. [23] at the test rig. For numerical calculations we use the parameters of the corresponding disk brake throughout the paper. We emphasize at this point that for the problem of brake squeal only angular velocities up to 4000 rpm are physically relevant, which corresponds to a dimensionless $\Omega = 2.3 \times 10^{-2}$. In other applications much larger dimensionless angular velocities arise.

The horizontal lines in Fig. 5 for m=0 are umbrella modes of the plate. The spectrum of the reduced two-dimensional system corresponding to $m > 0$ is simple, except at the critical velocities

$$\Omega_1^c = 0, \quad \lambda_1^{c\pm} = \pm i\omega_{mn}$$

$$\Omega_2^c = \frac{1}{m}\omega_{mn}, \quad \lambda_2^{c\pm} = 0$$

where it is seen to be semisimple by calculating the corresponding eigenvectors. Note that additional crossings of eigenvalues occurring in the spectrum are semisimple as well, which follows from the decoupling of the matrices. Qualitatively it agrees with other results obtained in literature especially with the observation made in Ref. [24].

4.1.2 Disk. The spectrum for the unperturbed problem of the disk was calculated by Chen and Jhu in Ref. [16] using Lame potentials. Since it is numerically difficult to solve the characteristic equation, in this paper we prefer to calculate the spectrum using a Ritz discretization approach. The results obtained with the Ritz method have been validated by comparison to the results in Refs. [25,16]. The energy expressions from Eq. (19) corresponding to the disk equations are discretized using

$$u(r,\varphi) = \sum_{m=0}^{\hat{m}} \sum_{n=1}^{\hat{n}} \left[\sin\left(\frac{n\pi(r-r_i)}{2(r_o-r_i)} \right) \cos m\varphi \right] q_{mn}^{uc}(t) + \sum_{m=1}^{\hat{m}} \sum_{n=1}^{\hat{n}} \left[\sin\left(\frac{n\pi(r-r_i)}{2(r_o-r_i)} \right) \sin m\varphi \right] q_{mn}^{us}(t) \tag{79}$$

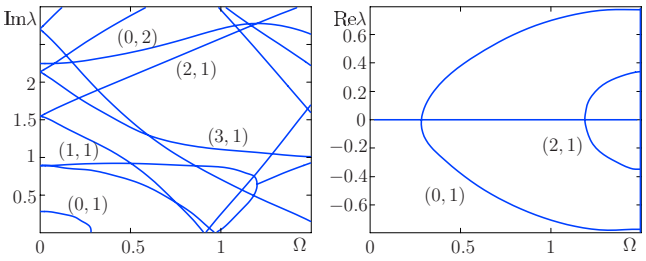

Fig. 6 Spectrum of the in-plane vibrations of the unperturbed problem (disk) for r_i=0.153

$$v(r,\varphi) = \sum_{m=0}^{\hat{m}} \sum_{n=1}^{\hat{n}} \left[\sin\left(\frac{n\pi(r-r_i)}{2(r_o-r_i)} \right) \cos m\varphi \right] q_{mn}^{vc}(t) + \sum_{m=1}^{\hat{m}} \sum_{n=1}^{\hat{n}} \left[\sin\left(\frac{n\pi(r-r_i)}{2(r_o-r_i)} \right) \sin m\varphi \right] q_{mn}^{vs}(t) \tag{80}$$

which can be seen to form a base for the problem, since they satisfy the geometric boundary conditions and since the trigonometric functions are known to be complete. Carrying out the variations in Eq. (19) over the functions q_{mn}^{ij}, we obtain the equations of motion

$$\boldsymbol{M}\ddot{\boldsymbol{q}} + \boldsymbol{G}\dot{\boldsymbol{q}} + \boldsymbol{K}\boldsymbol{q} = \boldsymbol{0} \tag{81}$$

of the unperturbed problem, where $\boldsymbol{M}$ and $\boldsymbol{K}$ are symmetric and $\boldsymbol{G}$ is skew-symmetric. The corresponding eigenvalue problem reads

$$[\boldsymbol{M}\lambda^2 + \boldsymbol{G}\lambda + \boldsymbol{K}] \begin{bmatrix} \boldsymbol{u} \\ \boldsymbol{v} \end{bmatrix} = \boldsymbol{0} \tag{82}$$

where

$$\boldsymbol{u} = [q_{01}^{uc}, q_{01}^{us}, \ldots, q_{\hat{m}\hat{n}}^{uc}, q_{\hat{m}\hat{n}}^{us}]^T \tag{83}$$

$$\boldsymbol{v} = [q_{01}^{vc}, q_{01}^{vs}, \ldots, q_{\hat{m}\hat{n}}^{vc}, q_{\hat{m}\hat{n}}^{vs}]^T \tag{84}$$

and yields the spectrum depicted in Fig. 6.

At Ω=0.28 the (0,1) eigenform of the system loses stability by divergence (we use again the notation (m,n), where as for the plate m denotes the number of nodal diameters and n denotes the number of nodal circles). The system exhibits flutter at Ω=1.2.

4.2 Perturbation Formulas. For the following perturbation formulas we introduce the dimensionless parameters

$$\bar{r}_{pi} = 0.5988, \quad \bar{r}_{po} = 0.9444, \quad \varphi_p = 0.7$$

$$\bar{k} = 0.0093, \quad \bar{N}_0 = 6.4669 \times 10^{-6}, \quad \mu = 0.6$$

corresponding to a real disk brake [26,13]. We again skip the bar in the following for notational convenience. The weight function corresponding to the pads is chosen such that $\kappa(r,\varphi)=1$ if $(r,\varphi) \in B$, i.e., if (r,φ) are in the domain of the pad (denoted by B to be distinguished from the whole area of the plate surface denoted earlier by A) and $\kappa(r,\varphi)=0$ otherwise.

4.2.1 Plate. Expanding the perturbed eigenfunctions of the plate in terms of the eigenfunctions of the nonrotating plate and projection onto themselves yields

$$[\boldsymbol{M}\lambda^2 + (\boldsymbol{G} + \gamma\Delta\boldsymbol{G}^{\gamma} + \delta\Delta\boldsymbol{G}^{\delta})\lambda + \boldsymbol{K} + \gamma\Delta\boldsymbol{K}^{\gamma} + \delta\Delta\boldsymbol{K}^{\delta}]\boldsymbol{u} = 0 \tag{85}$$

where $\boldsymbol{M}$, $\boldsymbol{G}$, and $\boldsymbol{K}$ have been derived in Sec. 4.1.1 and

$$\Delta G_{ij}^{\gamma} = 0 \tag{86a}$$

$$\Delta G_{ij}^{\delta} = \int_B \frac{h^2 N_0 \mu}{2r\Omega} W^i_{,r} W^j_{,r} \mathrm{d}B \tag{86b}$$

$$\Delta K_{ij}^{\gamma} = \int_B \left[2kW^i W^j - \frac{hk\mu}{r} W^i_{,\varphi} W^j \right] \mathrm{d}B \tag{86c}$$

$$\Delta K_{ij}^{\delta} = \int_B \left[\mu^2 \frac{hN_0}{r^2} W^i_{,\varphi} W^j_{,\varphi} - \frac{h^2 N_0 \mu}{2r^2} W^i_{,r} W^j_{,\varphi} + \frac{h^2 N_0 \mu}{2r} W^i_{,r} W^j_{,r\varphi} \right] \mathrm{d}B \tag{86d}$$

are the perturbation matrices. Note that we have used integration by parts in some of the integrals and thereby eliminated transition terms originating from the discontinuity of the weight function $\kappa(r,\varphi)$. The matrices (86) are similar to the expressions one would have obtained from the Ritz discretization used in Ref. [13] taking into account an arbitrary number of shape functions. However, due to the reasons discussed in Sec. 3.4, the expressions obtained from the Ritz discretization contain a few more terms in ΔK_{ij}^{γ} and ΔK_{ij}^{δ}, which read

$$\Delta K_{ij}^{\gamma} = \int_B \left[2kW^i W^j - \frac{hk\mu}{r} W^i_{,\varphi} W^j \right] \mathrm{d}B \tag{87}$$

$$\Delta K_{ij}^{\delta} = \int_B \left[(1+\mu^2) \frac{hN_0}{r^2} W^i_{,\varphi} W^j_{,\varphi} - \frac{h^2 N_0 \mu}{2r^3} W^i_{,\varphi\varphi} W^j_{,\varphi} + \frac{h^2 N_0 \mu}{2r^2} (W^i_{,\varphi} W^j_{,r} - W^i_{,r} W^j_{,\varphi}) + hN_0 W^i_{,r} W^j_{,r} + \frac{h^2 N_0 \mu}{2r} (W^i_{,r} W^j_{,r\varphi} - W^i_{,\varphi r} W^j_{,r}) \right] \mathrm{d}B \tag{88}$$

It can be seen numerically that the additional terms are so small that they have practically no influence on the results.

The perturbation matrices are split into a symmetric and a skew-symmetric part

$$\boldsymbol{\Delta G}^{\gamma,\delta} = \boldsymbol{G}^{\gamma,\delta} + \boldsymbol{D}^{\gamma,\delta}, \quad \boldsymbol{G}^{\gamma,\delta} = -(\boldsymbol{G}^{\gamma,\delta})^T, \quad \boldsymbol{D}^{\gamma,\delta} = (\boldsymbol{D}^{\gamma,\delta})^T$$

$$\boldsymbol{\Delta K}^{\gamma,\delta} = \boldsymbol{K}^{\gamma,\delta} + \boldsymbol{N}^{\gamma,\delta}, \quad \boldsymbol{K}^{\gamma,\delta} = (\boldsymbol{K}^{\gamma,\delta})^T, \quad \boldsymbol{N}^{\gamma,\delta} = -(\boldsymbol{N}^{\gamma,\delta})^T$$

Using formula (61) for simple eigenvalues, we arrive at the expression

$$\lambda_1^{\gamma} = \frac{-\lambda_0 \bar{\boldsymbol{u}}^T \boldsymbol{\Delta G}^{\gamma} \boldsymbol{u} - \bar{\boldsymbol{u}}^T \boldsymbol{\Delta K}^{\gamma} \boldsymbol{u}}{2\lambda_0 \bar{\boldsymbol{u}}^T \boldsymbol{M} \boldsymbol{u} + \bar{\boldsymbol{u}}^T \boldsymbol{G} \boldsymbol{u}} = \frac{\omega^2 \bar{\boldsymbol{u}}^T \boldsymbol{\Delta G}^{\gamma} \boldsymbol{u} - i\omega \bar{\boldsymbol{u}}^T \boldsymbol{\Delta K}^{\gamma} \boldsymbol{u}}{\bar{\boldsymbol{u}}^T (-\boldsymbol{M}\omega^2 - \boldsymbol{K}) \boldsymbol{u}} = \frac{\omega^2 (\boldsymbol{a}^T \boldsymbol{D}^{\gamma} \boldsymbol{a} + \boldsymbol{b}^T \boldsymbol{D}^{\gamma} \boldsymbol{b}) + 2\omega \boldsymbol{a}^T \boldsymbol{N}^{\gamma} \boldsymbol{b} + i[2\omega^2 \boldsymbol{a}^T \boldsymbol{G}^{\gamma} \boldsymbol{b} + \omega(\boldsymbol{a}^T \boldsymbol{K}^{\gamma} \boldsymbol{a} + \boldsymbol{b}^T \boldsymbol{K}^{\gamma} \boldsymbol{b})]}{\boldsymbol{a}^T (-\boldsymbol{M}\omega^2 - \boldsymbol{K}) \boldsymbol{a} + \boldsymbol{b}^T (-\boldsymbol{M}\omega^2 - \boldsymbol{K}) \boldsymbol{b}} \tag{89}$$

where a and b are the real and imaginary parts of the eigenvector $\boldsymbol{u}_0$. To calculate λ_1^{δ} just replace γ with δ. From Eq. (89) we observe that for small γ and δ the stability behavior is determined by $\boldsymbol{D}^{\gamma,\delta}$ and $\boldsymbol{N}^{\gamma,\delta}$ only. Due to the decoupling of the equations for the unperturbed problem, only the 2×2 matrices having the same position in the perturbation matrices as the blocks corresponding to the eigenvalue of the unperturbed problem are relevant for the first term in the expansion of λ. The zeros in the corresponding eigenvector of the unperturbed problem suppress the influence of other terms. For the semisimple eigenvalues, more terms are relevant for the splitting of the double eigenvalue. From Eq. (63) it follows that λ_1^{ε} is determined from

$$\det \begin{bmatrix} c_1 \lambda_1^{\varepsilon} + a & b \\ c & c_2 \lambda_1^{\varepsilon} + d \end{bmatrix} = 0 \tag{90}$$

where

$$c_1 = 2\lambda_0 \bar{\boldsymbol{u}}_1^T \boldsymbol{M} \boldsymbol{u}_1 + \bar{\boldsymbol{u}}_1^T \boldsymbol{G} \boldsymbol{u}_1 \tag{91a}$$

$$c_2 = 2\lambda_0 \bar{\boldsymbol{u}}_2^T \boldsymbol{M} \boldsymbol{u}_2 + \bar{\boldsymbol{u}}_2^T \boldsymbol{G} \boldsymbol{u}_2 \tag{91b}$$

$$a = -\lambda_0 \bar{\boldsymbol{u}}_1^T \boldsymbol{\Delta G}^{\varepsilon} \boldsymbol{u}_1 - \bar{\boldsymbol{u}}_1^T \boldsymbol{\Delta K}^{\varepsilon} \boldsymbol{u}_1 \tag{91c}$$

$$b = -\lambda_0 \bar{\boldsymbol{u}}_1^T \boldsymbol{\Delta G}^{\varepsilon} \boldsymbol{u}_2 - \bar{\boldsymbol{u}}_1^T \boldsymbol{\Delta K}^{\varepsilon} \boldsymbol{u}_2 \tag{91d}$$

$$c = -\lambda_0 \bar{\boldsymbol{u}}_2^T \boldsymbol{\Delta G}^{\varepsilon} \boldsymbol{u}_1 - \bar{\boldsymbol{u}}_2^T \boldsymbol{\Delta K}^{\varepsilon} \boldsymbol{u}_1 \tag{91e}$$

$$d = -\lambda_0 \bar{\boldsymbol{u}}_2^T \boldsymbol{\Delta G}^{\varepsilon} \boldsymbol{u}_2 - \bar{\boldsymbol{u}}_2^T \boldsymbol{\Delta K}^{\varepsilon} \boldsymbol{u}_2 \tag{91f}$$

We obtain

$$\lambda_1^{\varepsilon} = \frac{-(dc_1 + ac_2) \pm \sqrt{(dc_1 - ac_2)^2 + 4c_1 c_2 cb}}{2c_1 c_2} \tag{92}$$

which shows that in the generic case, when the expression under the square root does not vanish, avoided crossings of imaginary parts and imperfect merging of modes occur as depicted in Fig. 7, where we used the $\delta=3$ and $\gamma=3$ for the pads. Since

$$\frac{\|\Delta \boldsymbol{K}^{\gamma}\|_F}{\|\boldsymbol{K}_0\|_F} = 0,\ 0491, \quad \frac{\|\Delta \boldsymbol{G}^{\gamma}\|_F}{\|\boldsymbol{K}_0\|_F} = 0, \quad \frac{\|\Delta \boldsymbol{K}^{\delta}\|_F}{\|\boldsymbol{K}_0\|_F} = 1.618 \times 10^{-6}$$

$$\frac{\|\Delta \boldsymbol{G}^{\delta}\|_F}{\|\boldsymbol{K}_0\|_F} = \frac{1.306 \times 10^{-6}}{\Omega}, \quad \boldsymbol{K}_0 = \boldsymbol{K}|_{\Omega=0}$$

where $\|\cdot\|_F$ stands for the Frobenius norm, even the perturbations $\gamma\Delta\boldsymbol{K}^{\gamma} + \delta\Delta\boldsymbol{K}^{\delta}$ and $\gamma\Delta\boldsymbol{G}^{\gamma} + \delta\Delta\boldsymbol{G}^{\delta}$ can be considered small for speed ranges not too close to $\Omega=0$ (cf. also Fig. 11).

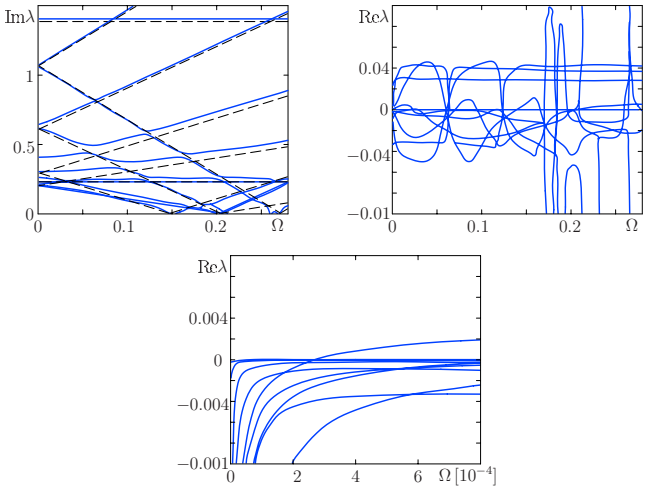

Fig. 7 Spectrum of the perturbed plate problem for $\gamma=\delta=3$. Dashed lines: unperturbed problem; lower plot: zoom for small Ω.

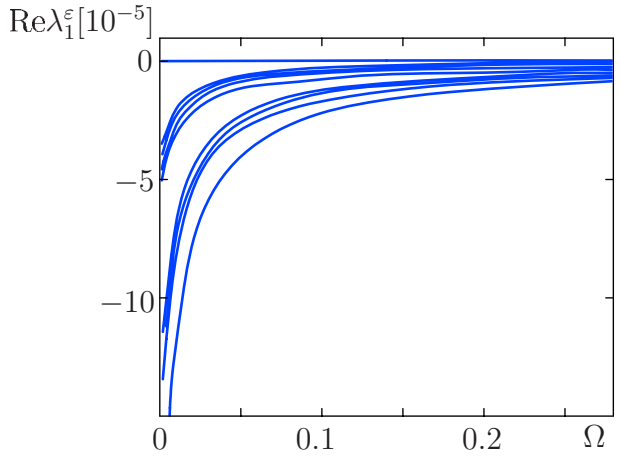

Fig. 8 λ_1^ε for the perturbed disk problem for r_i=0.153

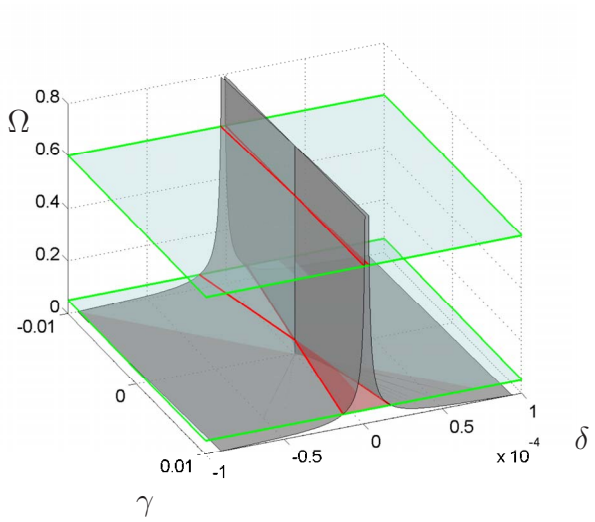

Fig. 9 Three-dimensional stability boundaries

Generic pictures for avoided crossings have been derived in Ref. [27] for the matrix case. In our case they look similar, except for the fact that we have a vanishing real part for all eigenvalues in the unperturbed problem. We see that the combined action of the dissipative and nonconservative positional forces moves some of the eigenvalues to the right side of the complex plane for the values of Ω not exceeding the first critical speed. For the parameters considered in Fig. 7 the system gets unstable at a dimensionless $\Omega=2.7\times10^{-4}$, which for the physical disk brake studied corresponds to an angular velocity of about 46 rpm. Therefore, the application of the brake pads to the disk can cause flutter instability in the subcritical range, which is typical for squeal.

4.2.2 Disk. According to Eq. (61), for simple eigenvalues of the unperturbed problem the first term in the expansion (60) reads

$$\lambda_1^\varepsilon = \frac{\displaystyle\int_B \left[\frac{2\mu N_0 h}{r\Omega}\bar{u}u + \frac{2\mu N_0 h}{r}\bar{u}u - \frac{2\mu N_0 h}{r}\bar{u}v\right]\mathrm{d}B}{\displaystyle\int_A [2\lambda(u\bar{u}+v\bar{v}) + 2\Omega[\bar{u}(u_{,\varphi}-v)+\bar{v}(u+v_{,\varphi})]]\mathrm{d}A} \tag{93}$$

Substituting the eigenfunctions obtained from the Ritz method $u=\boldsymbol{U}\boldsymbol{u}$ and $v=\boldsymbol{V}\boldsymbol{v}$, where $\boldsymbol{U}$ and $\boldsymbol{V}$ are row matrices containing the shape functions for u and v, and $[\boldsymbol{u}^T,\boldsymbol{v}^T]^T$ is the eigenvector corresponding to Eq. (82), yields

$$\lambda_1^\varepsilon = \frac{-\lambda_0\begin{bmatrix}\bar{\boldsymbol{u}}^T & \bar{\boldsymbol{v}}^T\end{bmatrix}\boldsymbol{\Delta G}^\delta\begin{bmatrix}\boldsymbol{u}\\ \boldsymbol{v}\end{bmatrix} - \begin{bmatrix}\bar{\boldsymbol{u}}^T & \bar{\boldsymbol{v}}^T\end{bmatrix}\boldsymbol{\Delta K}^\delta\begin{bmatrix}\boldsymbol{u}\\ \boldsymbol{v}\end{bmatrix}}{2\lambda_0\begin{bmatrix}\bar{\boldsymbol{u}}^T & \bar{\boldsymbol{v}}^T\end{bmatrix}\boldsymbol{M}\begin{bmatrix}\boldsymbol{u}\\ \boldsymbol{v}\end{bmatrix} + \begin{bmatrix}\bar{\boldsymbol{u}}^T & \bar{\boldsymbol{v}}^T\end{bmatrix}\boldsymbol{G}\begin{bmatrix}\boldsymbol{u}\\ \boldsymbol{v}\end{bmatrix}} \tag{94}$$

which coincides with the perturbation formulas one would have obtained by perturbing the discretized eigenvalue problem (82). The first correction terms from Eq. (60) for simple eigenvalues of the perturbed disk problem are shown in Fig. 8 for the real part.

We observe that in the range below the first critical speed $\mathrm{Re}(\lambda_1^\varepsilon)$ is strictly negative. For $\Omega\to0$ the real parts become infinite, which can be explained by the term proportional to $1/\Omega$ in the damping matrix. For the semisimple eigenvalues we expect the same behavior, since the eigenvalues of a matrix polynomial depend continuously on the matrix entries.

4.3 Stability Boundaries. In Sec. 4.2.1 we derived formulas for the change in simple and semisimple eigenvalues occurring in the spectrum of the unperturbed plate problem caused by small changes in the parameters. For a fixed rotational speed of the plate, the stable region in the parameter plane γ,δ is given by those areas where all eigenvalues of the problem have a nonpositive real part. For each simple purely imaginary eigenvalue of the unperturbed problem λ_j there is a stable region, which in the first approximation is the half plane

$$\gamma\,\mathrm{Re}(\lambda_1^{j\gamma}) + \delta\,\mathrm{Re}(\lambda_1^{j\delta}) \le 0, \quad \forall\, j \tag{95}$$

At a fixed rotational speed Ω, where all eigenvalues are simple, the stability region in the γ,δ plane is given by the intersection of the half-planes defined in Eq. (95). Depending on the parameters, it can be a sector limited by an angle, a line (for $\mathrm{Re}(\lambda_1^{1\gamma})/\mathrm{Re}(\lambda_1^{1\delta})=\cdots=\mathrm{Re}(\lambda_1^{n\gamma})/\mathrm{Re}(\lambda_1^{n\delta})$) or just the point $\gamma=\delta=0$. Approximations to the stability boundary therefore coincide with the lines

$$\gamma = -\frac{\mathrm{Re}(\lambda_1^{1\delta})}{\mathrm{Re}(\lambda_1^{1\gamma})}\delta = -\frac{\omega(\boldsymbol{a}^T\boldsymbol{D}^\delta\boldsymbol{a}+\boldsymbol{b}^T\boldsymbol{D}^\delta\boldsymbol{b})+2\boldsymbol{a}^T\boldsymbol{N}^\delta\boldsymbol{b}}{\omega(\boldsymbol{a}^T\boldsymbol{D}^\gamma\boldsymbol{a}+\boldsymbol{b}^T\mathbf{D}^\gamma\boldsymbol{b})+2\boldsymbol{a}^T\boldsymbol{N}^\gamma\boldsymbol{b}}\delta \tag{96}$$

Again, recall $\boldsymbol{u}=\boldsymbol{a}+i\boldsymbol{b}$. For the two-dimensional system of the plate corresponding to its (3,1) mode, the stability boundaries are depicted in Fig. 9, where only the areas with positive γ and δ are physically meaningful.

From Fig. 9 one expects that for $\Omega\to0$ the stable region coincides with the half plane $\Omega=0,\delta>0$ and for $\Omega\to\infty$ the stable region is a line. It is not difficult to verify this analytically.

Consider the case $\Omega\to0$. In this case $d_{11}^\delta\to\infty$ and consequently in Eq. (96) the numerator tends to infinity since always two eigenvectors of the unperturbed system with nonvanishing first component of $\boldsymbol{a}$ or $\boldsymbol{b}$ can be found (the eigenvectors of a purely gyroscopic system span the solution space provided that $\boldsymbol{M}$ and $\boldsymbol{K}$ are positive definite). The stability boundary is therefore given by $\delta=0$.

Now consider the case $\Omega\to\infty$. We will show that in the limit the eigenvectors corresponding to the pairs of eigenvalues (76) coincide and Eq. (96) yields the same expression for each eigenvalue. We note that for increasing Ω the relative difference between λ^1 and λ^2 tends to zero, i.e.,

$$\lim_{\Omega\to\infty}\Delta\lambda = \lim_{\Omega\to\infty}\frac{\lambda^1-\lambda^2}{\lambda^1} = 0 \tag{97}$$

as we can see from Eq. (76). Consider the matrix $\boldsymbol{A}$ describing Eq. (76) written as a first order system with eigenvectors $\boldsymbol{v}_1$ and $\boldsymbol{v}_2$ corresponding to λ^1 and λ^2, i.e.,

$$\boldsymbol{A}\boldsymbol{v}_1 = \lambda^1\boldsymbol{v}_1 \tag{98}$$

$$\boldsymbol{A}\boldsymbol{v}_2 = \lambda^2\boldsymbol{v}_2 \tag{99}$$

Using Eq. (97) we obtain

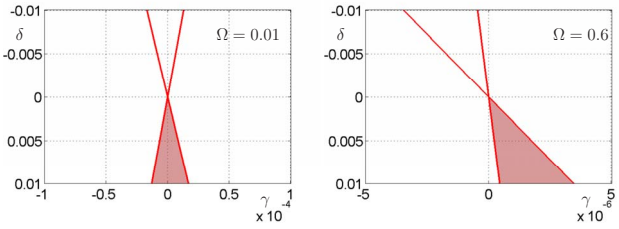

Fig. 10 Stability boundaries in the sub- and supercritical ranges

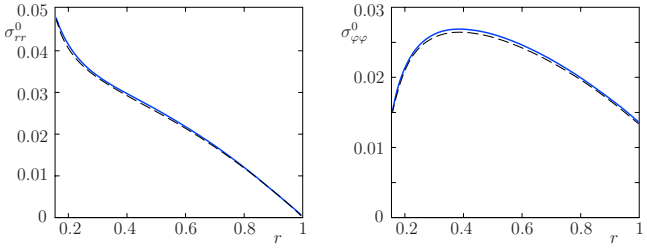

Fig. 12 Prestress due to rotation of the disk ($\Omega=0.28$)

$$\boldsymbol{A}(\boldsymbol{v}_1-\boldsymbol{v}_2)=\lambda^1(\boldsymbol{v}_1-\boldsymbol{v}_2)+\Delta\lambda\boldsymbol{v}_2 \tag{100}$$

$$\boldsymbol{A}(\boldsymbol{v}_2-\boldsymbol{v}_1)=\lambda^2\left(\boldsymbol{v}_2-\frac{1}{1-\Delta\lambda}\boldsymbol{v}_1\right) \tag{101}$$

which by addition and taking the limit $\Delta\lambda\to 0$ yields

$$(\lambda^1-\lambda^2)(\boldsymbol{v}_1-\boldsymbol{v}_2)=0 \tag{102}$$

and hence $\boldsymbol{v}_1=\boldsymbol{v}_2$.

From the above reasoning taking into account that the stable lines for different pairs of eigenvalues have different slopes we conclude that the system definitely becomes unstable for some Ω.

A second fact to be observed from Fig. 10 is that in the supercritical range damping can have a destabilizing effect, which agrees with the results of Ref. [28]. In view of the Thompson–Tait–Chetaev theorem [29] this effect is not surprising, although this theorem is not directly applicable, since the forces originating from the prestress N_0 are not purely dissipative.

We stress that the approximations for the stability boundaries are only valid for small perturbations. In Fig. 11 they are compared with numerical calculations of the eigenvalues at particular points in the parameter space. In the vicinity of the unperturbed problem they are seen to give good approximations.

4.4 The Effect of Centrifugal Stiffening in the Plate Equations. In this section we discuss how the effect of centrifugal stiffening enters into the plate vibrations and compare the results with the ones obtained in Secs. 4.2 and 4.3. Using the assumption that $u_{,x}$, $u_{,y}$, $v_{,x}$, and $v_{,y}$ occurring in Eq. (29) are of the order of magnitude of $w_{,x}^2$ and $w_{,y}^2$ and neglecting terms containing z^2 since the plate is thin [3] we obtain

$$e_{xx}=u_{,x}-zw_{,xx}+\tfrac{1}{2}w_{,x}^2 \tag{103a}$$

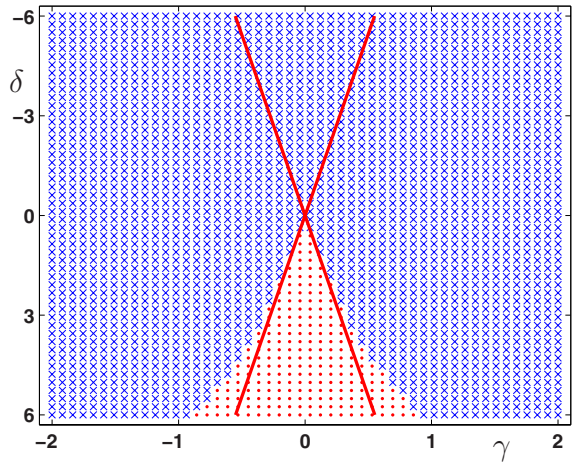

Fig. 11 Comparison of analytical and numerical results for $\Omega=10^{-3}$ (dot: stable; cross: unstable)

$$e_{yy}=v_{,y}-zw_{,yy}+\tfrac{1}{2}w_{,y}^2 \tag{103b}$$

$$e_{zz}=0 \tag{103c}$$

$$e_{xy}=\tfrac{1}{2}u_{,y}+\tfrac{1}{2}v_{,x}-zw_{,xy}+\tfrac{1}{2}w_{,y}w_{,x}, \tag{103d}$$

$$e_{yz}=0 \tag{103e}$$

$$e_{xz}=0 \tag{103f}$$

Deriving the equations of motion from the principle of virtual work under consideration of the prestress of the disk due to the rotation and transformation into polar coordinates after linearization yields

$$\rho h w_{,tt}+2h\rho\Omega w_{,t\varphi}+\Omega^2\rho h w_{,\varphi\varphi}-\frac{1}{r}\frac{\partial}{\partial r}(rh\sigma_{rr}^0 w_{,r})-\frac{h\sigma_{\varphi\varphi}^0}{r^2}w_{,\varphi\varphi}$$

$$+D\nabla^4 w=F_z-\frac{1}{r}T_{r,\varphi}+T_{\varphi,r} \tag{104}$$

where the boundary conditions are as previously given by Eq. (38) and σ_{rr}^0 and $\sigma_{\varphi\varphi}^0$ are the prestresses of the disk in radial and circumferential directions, which will be calculated in the sequel. We remark that due to the rotational symmetry of the plate $\sigma_{r\varphi}^0=0$.

4.4.1 Calculation of the Prestress. The prestress originating from the rotation is calculated by finding a stationary solution for Eq. (40) with $\kappa=0$ from which the strain can be calculated. The prestress can then be found from the stress-strain relations. Due to the symmetry of the disk it is clear that σ_{rr}^0 and $\sigma_{\varphi\varphi}^0$ depend on r only and that $v=0$. In dimensionless form the resulting differential equation reads

$$\left(\frac{\partial^2}{\partial r^2}+\frac{1}{r}\frac{\partial}{\partial r}+(1-\nu^2)\Omega^2-\frac{1}{r^2}\right)u=-(1-\nu^2)\Omega^2 r \tag{105}$$

with boundary conditions

$$u|_{r_i}=0,\quad \left(\frac{\partial}{\partial r}+\nu\frac{1}{r}\right)u|_{r=r_o}=0 \tag{106}$$

The boundary value problem for the ordinary differential equation (105) with boundary condition (106) coincides with the one obtained in Ref. [30] by linearization of the boundary value problem obtained using the nonlinear deformation gradient. The general solution of Eq. (105) is given by

$$u(r)=C_1J_1(r\sqrt{\Omega^2(1-\nu^2)})+C_2Y_1(r\sqrt{\Omega^2(1-\nu^2)})-r \tag{107}$$

as derived in Ref. [30] where J_1 and Y_1 are the well known Bessel functions of the first and second kinds. The constants C_1 and C_2 are obtained by adjusting Eq. (107) to the boundary condition (106). For the dimensionless angular velocity $\Omega=0.28$ the resulting $\sigma_{rr}^0(r)$ and $\sigma_{\phi\phi}^0(r)$ are plotted in Fig. 12 as solid lines.

For small angular velocities Ω the term proportional to Ω^2 in Eq. (105) can be neglected. The corresponding result was derived in Ref. [31] using first order theory, where also the solution for the

simplified boundary value problem for the corresponding ordinary differential equation is given. The prestress can then be calculated from the stress-strain relations as

$$\sigma_{rr}^0(r) = \left(a_1 + \frac{a_2}{r^2} - \frac{3+\nu}{8}r^2\right)\Omega^2 \tag{108}$$

$$\sigma_{\varphi\varphi}^0(r) = \left(a_1 - \frac{a_2}{r^2} - \frac{1+3\nu}{8}r^2\right)\Omega^2 \tag{109}$$

where

$$a_1 = \left(\frac{1+\nu}{8}\right)\frac{(3+\nu)+(1-\nu)\left(\frac{r_i}{r_o}\right)^4}{(1-\nu)\left(\frac{r_i}{r_o}\right)^2+(1+\nu)} \tag{110}$$

$$a_2 = \left(\frac{1-\nu}{8}\right)\frac{(3+\nu)\left(\frac{r_i}{r_o}\right)^2+(1+\nu)\left(\frac{r_i}{r_o}\right)^4}{(1-\nu)\left(\frac{r_i}{r_o}\right)^2+(1+\nu)} \tag{111}$$

for the boundary condition (106). The expression for prestress given by Eq. (108) is easier to handle in numerical calculations since Ω appears polynomially and not as the argument of a Bessel function as in Eq. (105). The corresponding prestress is plotted in Fig. 12 by the dashed lines for $\Omega=0.28$. Since it is seen from Fig. 12 that for the rotational speeds considered in this paper Eq. (108) is a very good approximation, all numerical calculations for the plate are carried out with these equations. For larger Ω Eq. (108) is no longer valid and it cannot be used to determine static instabilities as is done in Ref. [30] using Eq. (107).

4.4.2 Results From the Perturbation Analysis. Performing a perturbation analysis on the prestressed plate analogous to the investigations performed in Secs. 4.2 and 4.3 previous sections one at first has to calculate the spectrum of the unperturbed problem. The only differences in the unperturbed boundary value problems are the terms proportional to $\sigma_{rr}^0(r)$ and $\sigma_{\phi\phi}^0(r)$. Expanding the eigenfunctions of the unperturbed problem in terms of eigenfunctions of the nonrotating plate as in Eq. (76) and projecting onto them one sees by similar argument as in Sec. 4.1 that equations corresponding to different nodal diameters m will decouple. Due to the dependence of $\sigma_{rr}^0(r)$ and $\sigma_{\phi\phi}^0(r)$ on r a further decoupling does not occur.

The spectrum of the unperturbed problem resulting from the Ritz approach using the ten lowest eigenmodes of the nonrotating plate is given in Fig. 13 by the solid lines.

The dashed lines show the spectrum neglecting the influence of the prestress and one can observe the stiffening effect since the eigenfrequencies increase. The eigenvalues for the perturbed problem using the same shape functions in a Ritz approach for the perturbed problem are shown in Fig. 14.

The perturbation formulas are similar to Eq. (89) but larger matrices and eigenvectors have to be used since equations corresponding to the same nodal diameter in the unperturbed problem are coupled. We see that there is no qualitative difference to the graphs obtained neglecting the prestress. The same holds true for the stability boundaries; therefore they are not redrawn for the prestressed case.

5 Nonlinear Analysis

When dealing with linear models, in case of an instability of the trivial solution, the amplitudes of the vibration become infinite. In practice this does not happen, since nonlinearities limit the amplitudes. In this section we therefore introduce a nonlinear stiffness characteristic in the pads and investigate the discretized equations of motion using the continuation method. We concentrate on the disk brake model with parameters given in Sec. 4.2. Since it is

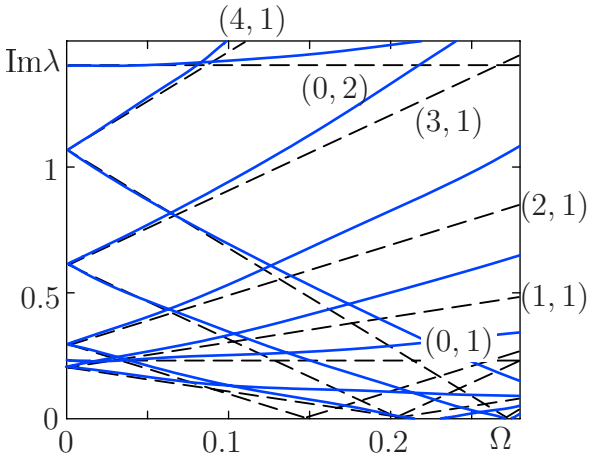

Fig. 13 Spectrum of the out-of-plane vibrations of the unperturbed problem (prestressed plate) for r_i=0.154 (spectral mesh)

observed in the laboratory that the squealing brake rotor almost vibrates in the first pair of eigenmodes of the nonrotating plate, we limit the expansion of the solution to these modes, i.e.,

$$w(r,\varphi,t) = R_{mn}(r)(q_1(t)\cos m\varphi + q_2(t)\sin m\varphi) \tag{112}$$

where $R_{mn}(r)$ is the radial component of an eigenfunction of the corresponding nonrotating plate. As before, the quantities m and n denote the number of nodal diameters and nodal circles, respectively. Note that all boundary conditions of the rotating plate are satisfied by the shape functions. The derivation of the equations of motion made clear that nonlinear kinematics, i.e., using the nonlinear deformation gradient, yields equations that are highly coupled. Since we expect the amplitude of the disk to be very small, we stick to the assumption of linear kinematics and assume that nonlinearities only enter the system through a nonlinear pad stiffness. Considering this nonlinearity of the pads, the force balance at the upper brake pad (16) now reads

$$(\boldsymbol{N}_{\bar{P}} + \boldsymbol{R}_{\bar{P}}) \cdot \boldsymbol{e}_z + N_0 - F_{\bar{P}} = 0 \tag{113}$$

where

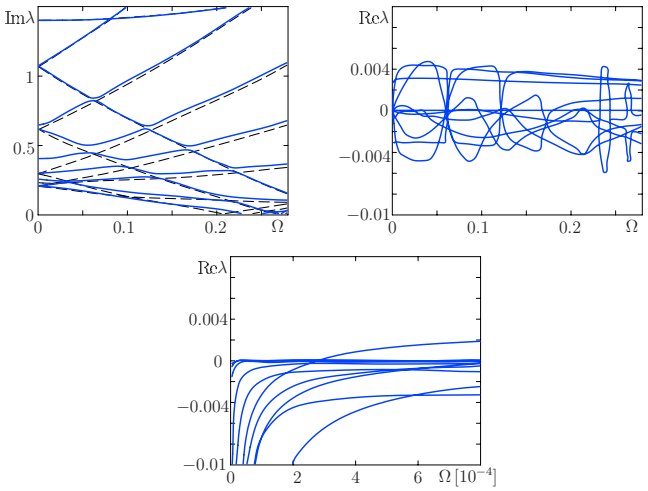

Fig. 14 Spectrum of the perturbed plate problem for $\gamma=\delta=3$. Dashed lines: unperturbed problem; lower plot: zoom for small Ω.

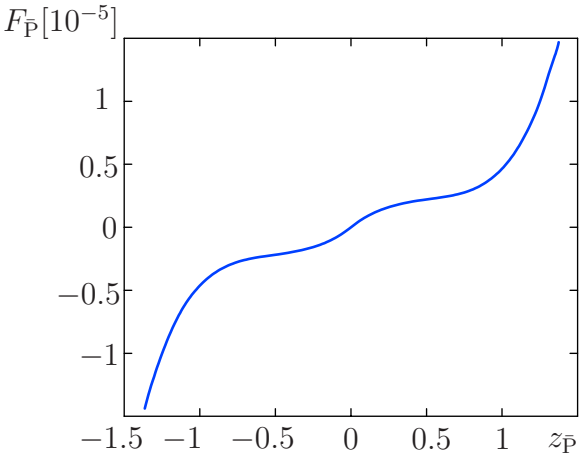

Fig. 15 Stiffness characteristic

$$F_{\bar{P}} = k_1\left(z_{\bar{P}} + \frac{h}{2}\right) + \mathrm{sgn}\left(z_{\bar{P}} + \frac{h}{2}\right)k_2\left(z_{\bar{P}} + \frac{h}{2}\right)^2 + k_3\left(z_{\bar{P}} + \frac{h}{2}\right)^3 + k_5\left(z_{\bar{P}} + \frac{h}{2}\right)^5 \tag{114}$$

and the sign function ensures that the stiffness characteristic is point-symmetric with respect to the prestressed configuration.

Very little is known about the stiffness and damping parameters of the pads; therefore the minimal model can only be investigated qualitatively. For a bifurcation analysis using AUTO [32] the stiffness and damping parameters are varied in a physically plausible range. Depending on the parameters we obtain a subcritical or a supercritical Hopf bifurcation when increasing the rotational speed of the disk.

Using the dimensionless stiffness parameters

$$k_1 = 0.0093, \quad k_2 = -1.30 \times 10^5, \quad k_3 = 4.69 \times 10^{11}, \quad k_5 = 2.21 \times 10^{22} \tag{115}$$

we obtain the stiffness characteristic shown in Fig. 15 and the bifurcation diagram in Fig. 16.

The phenomenon of a subcritical Hopf bifurcation has been observed in the laboratory. When accelerating the disk, squeal arises only above a certain angular velocity, but when the squealing brake is decelerated squeal is observed almost until the disk comes to a complete rest. However, we remark that this characteristic, i.e., the range of speed, is much smaller in the present model than one would have expected from laboratory experiments. This is most likely due to the fact that a minimal model is investigated and adjacent parts of the disk brake are not taken into account. Nevertheless the characteristic effect can be observed in the phenomenological model (cf. Fig. 16).

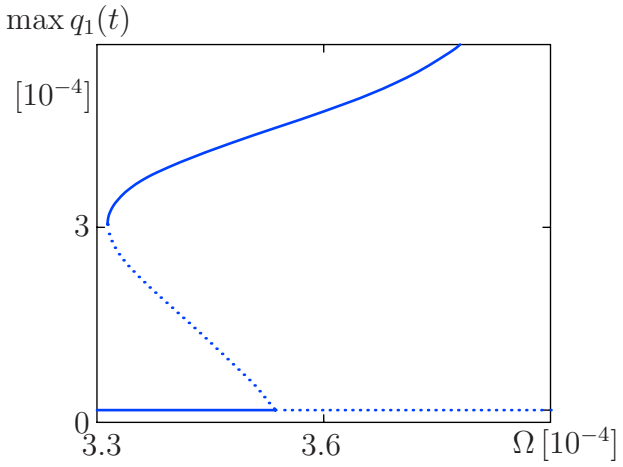

Fig. 16 Bifurcation diagram

6 Conclusion

This paper investigates the stretching and bending of an annular Kirchhoff plate in frictional contact with idealized distributed pads. The model of the pads is rather flexible to be employed in a variety of problems including clutches. The equations of motion are derived from the basics of the theory of elasticity and coupling between disk and plate equations is carefully examined. Under the assumptions used in this paper, the disk and the plate equations are decoupled in the linear case. Using perturbation techniques, it is shown that at least in the subcritical range for parameters of a brake disk the plate equations determine the stability behavior of the system. Subcritical flutter instability is observed caused by the combined action of dissipative and nonconservative positional forces. Approximations to the stability boundaries of the system are calculated from the perturbation formulas. The interpretation of the problem as a perturbation problem provides an effective tool for the stability analysis.

Finally, a nonlinear analysis of the discretized plate equations is performed to investigate the influences of the nonlinearities originating from the friction material. Observations of nonlinearities made at a squealing disk brake at the test rig, which have not been investigated in literature, can be verified qualitatively from the theoretical model using the continuation method.

Although plate and disk equations decouple in the linear case, i.e., the stability behavior is determined by the plate equations only, they are coupled through nonlinear terms. An instability in the plate equations is an instability of the complete system since the disk equations are excited through nonlinear terms. Consequently the squealing brake will show in- and out-of-plane vibrations as seen from experiments.

Acknowledgment

The work was partly supported by the Alexander von Humboldt-Foundation and DFG Grant No. HA 1060/43-1.

References

[1] Lamb, H., and Southwell, R., 1921, "The Vibrations of a Spinning Disk," Proc. R. Soc. London, Ser. A, **99**, pp. 272–280.
[2] Southwell, R., 1922, "On the Free Transverse Vibrations of a Uniform Circular Disc Clamped at Its Centre; and on the Effects of Rotation," Proc. R. Soc. London, Ser. A, **101**, pp. 133–153.
[3] Washizu, K., 1974, *Variational Methods in Elasticity and Plasticity*, Pergamon, New York.
[4] Baddour, N., and Zu, J., 2001, "A Revisit of Spinning Disk Models. Part I: Derivation of Equations of Motion," Appl. Math. Model., **25**, pp. 541–559.
[5] Baddour, N., and Zu, J., 2001, "A Revisit of Spinning Disk Models. Part II: Linear Transverse Vibrations," Appl. Math. Model., **25**, pp. 561–578.
[6] Moser, F., Fischer, M., and Rumold, W., 2002, "Dreidimensionale Messung von Betriebsschwingformen quietschender Scheibenbremsen," VDI-Ber., **1736**, pp. 71–83.
[7] Mottershead, J., 1998, "Vibration- and Friction-Induced Instability in Disks," Shock Vib. Dig., **30**(1), pp. 14–31.
[8] Ono, H., Chen, J., and Bogy, D. B., 1991, "Stability Analysis for the Head-Disk Interface in a Flexible Disk Drive," ASME J. Appl. Mech., **58**, pp. 1005–1014.
[9] Ouyang, H., and Mottershed, J. E., 2004, "Dynamic Instability of an Elastic Disk Under the Action of a Rotating Friction Couple," ASME J. Appl. Mech., **71**, pp. 753–758.
[10] Kinkaid, N. M., O'Reilly, O. M., and Papadopoulos, P., 2003, "Automotive Disc Brake Squeal," J. Sound Vib., **267**, pp. 105–166.
[11] Ibrahim, R. A., 1994, "Friction-Induced Vibration, Chatter, Squeal and Chaos, Part I: Mechanics of Contact and Friction," Appl. Mech. Rev., **47**(7), pp. 227–253.
[12] Tseng, J. G., and Wickert, J. A., 1998, "Nonconservative Stability of a Friction Loaded Disk," ASME J. Vibr. Acoust., **120**, pp. 922–929.
[13] Hochlenert, D., Spelsberg-Korspeter, G., and Hagedorn, P., 2007, "Friction Induced Vibrations in Moving Continua and Their Application to Brake Squeal," ASME J. Appl. Mech., **74**, pp. 542–549.
[14] Kirillov, O. N., and Seyranian, A. P., 2004, "Collapse of the Keldysh Chains

and Stability of Continuous Nonconservative Systems," SIAM J. Appl. Math., **64**(4), pp. 1383–1407.
[15] Seyranian, A. P., and Kliem, W., 2001, "Bifurcations of Eigenvalues of Gyroscopic Systems With Parameters Near Stability Boundaries," ASME J. Appl. Mech., **68**, pp. 199–205.
[16] Chen, J. S., and Jhu, J. L., 1996, "On the In-Plane Vibration and Stability of a Spinning Annular Disk," J. Sound Vib., **195**(4), pp. 585–593.
[17] Hagedorn, P., 1986, "Eine Bemerkung zur Momentenimpedanz bei Plattenschwingungen in der Substrukturtechnik," ZAMP, **37**, pp. 293–303.
[18] Vishik, M. I., and Lyusternik, L. A., 1960, "The Solution of Some Perturbation Problems for Matrices and Selfadjoint or Non-Selfadjoint Differential Equations I," Russ. Math. Surveys, **15**, pp. 1–73.
[19] Vishik, M. I., and Lyusternik, L. A., 1960, "The Asymptotic Behaviour of Solutions of Linear Differential Equations With Large or Quickly Changing Coefficients and Boundary Conditions," Russ. Math. Surveys, **15**, pp. 23–91.
[20] Vidoli, S., and Vestroni, F., 2005, "Veering Phenomena in Systems With Gyroscopic Coupling," ASME J. Appl. Mech., **72**, pp. 641–647.
[21] Leissa, A., 1969, "Vibrations of Plates," NASA, Report No. SP-160.
[22] Günther, U., and Kirillov, O. N., 2006, "Krein Space Related Perturbation Theory for MHD α^2-Dynamos and Resonant Unfolding of Diabolical Points," J. Phys. A, **39**, pp. 10057–10076.
[23] Jearsiripongkul, T., 2005, "Squeal in Floating Caliper Disk Brakes: A Mathematical Model," Ph.D. thesis, Technische Universität Darmstadt, Darmstadt, Germany.
[24] Renshaw, A. A., and Mote, C. D., 1992, "Absence of One Nodal Diameter Critical Speed Modes in an Axisymmetric Rotating Disk," Trans. ASME, J. Appl. Mech., **59**, pp. 687–688.
[25] Chen, J.-S., and Jhu, J.-L., 1996, "In-Plane Response of a Rotating Annular Disk Under Fixed Concentrated Edge Loads," Int. J. Mech. Sci., **38**(12), pp. 1285–1293.
[26] Hochlenert, D., 2006, "Selbsterregte Schwingungen in Scheibenbremsen: Mathematische Modellbildung und aktive Unterdrückung von Bremsenquietschen," Ph.D. thesis, Technische Universität Darmstadt, Darmstadt, Germany.
[27] Kirillov, O., Mailybaev, A., and Seyranian, A., 2005, "Unfolding of Eigenvalue Surfaces Near a Diabolic Point Due to a Complex Perturbation," J. Phys. A, **38**(24), pp. 5531–5546.
[28] Kirillov, O. N., 2007, "Destabilization Paradox Due to Breaking the Hamiltonian and Reversible Symmetry," Int. J. Non-Linear Mech., **42**(1), pp. 71–87.
[29] Merkin, D. R., 1997, *Introduction to the Theory of Stability*, Springer, New York.
[30] Seemann, W., and Wauer, J., 1988, "Vibration of High Speed Disk Rotors," *Rotating Machinery Dynamics Proceedings of the Second International Symposium on Transport Phenomena and Dynamics of Rotating Machinery (ISROMAC-2)*.
[31] Timoshenko, S., and Goodier, J. N., 1951, *Theory of Elasticity*, McGraw-Hill, New York.
[32] Doedel, E., Pfaffenroth, R., Champneys, A., Fairgrieve, T., Kuznetsov, B. S., and Wang, X., 2001, "AUTO 2000: Continuation and Bifurcation Software for Ordinary Differential Equations (With HomCont)," California Institute of Technology, Technical Report.